Title
Morphodynamic stage threshold for confined mountain rivers can be identified using geomorphic covariance structure analysis

Authors
Pasternack, Gregory
Gore, Joni
Wiener, Jason

Publication Date
2021-10-10

DOI
10.1002/essoar.10508209.1

Title: Geomorphic covariance structure of a confined mountain river reveals landform organization stage threshold

Short title: Mountain river landform organization stage threshold

Authors: Gregory B. Pasternack*, Joni Gore, Jason Wiener

University of California, Davis, One Shields Avenue, Davis, CA 95616, USA

* Corresponding author. Tel.: +1 (530) 302-5658
E-mail: gpast@ucdavis.edu

Keywords*:* river topography, river classification, flow convergence routing, mountain rivers, fluvial geomorphology

Twitter: GCS analysis reveals mountain rivers have a flow threshold above which flow convergence routing morphodynamics governs landform organization

Cite as: Pasternack, G. B., Gore, J., Weiner, J. 2021. Geomorphic covariance structure of a confined mountain river reveals landform organization stage threshold. Earth Surface Processes and Landforms. DOI: 10.1002/esp.5195

This version of the article includes edits made during the galley proof stage, so it should have identical content as the publisher's version.

Abstract

Significant growth in mountain rivers research since 1990 has promoted the concept that canyon-confined mountain rivers have complex topographic features nested from base- to flood-stages due to canyon structure and abundant large bed elements. Nesting means literally structures inside of structures. Mathematically, nesting means that multiple individual features and repeating patterns exist at different frequency, amplitude, and phasing, and can be added together to obtain the complete structure. Until now, subreach-scale landform structure, including nesting, has not been quantified sufficiently to understand morphodynamic mechanisms that control and respond to such organization. Geomorphic covariance structure analysis offers a systematic framework for evaluating nested topographic patterns. In this study, a threshold stage in mountain river inundation was hypothesized to exist. Above this stage landform structure is organized to be freely self-maintaining via flow convergence routing morphodynamics. A 13.2 km segment of the canyon-confined Yuba River, California, was studied using 2944 cross-sections. Geomorphic covariance structure analysis was carried out on a meter-resolution topographic model to test the hypothesis. River width and bed elevation had significantly less variability than previously reported for lower slope, partially confined gravel/cobble river reaches. A critical stage threshold governing flow convergence routing morphodynamics was evident in several metrics. Below this threshold, narrow/high “nozzle” and wide/low “oversized” were the dominant landforms (excluding “normal channel”), while above it wide/high “wide bar” and narrow/low “constricted pool” were dominant. Three-stage nesting of base-bankfull-flood landforms

was dictated by canyon confinement, with nozzle-nozzle-nozzle nesting as the top permutation, excluding normal channel.

Introduction

In the 21st century geomorphologists have rapidly embraced systemic meter-scale mapping of landscapes (Bishop et al., 2012; Pasternack, 2019). Common procedures using such maps include river classification, spatially explicit hydrodynamic and morphodynamic modeling, and topographic change detection and analysis. These are used for many scientific and management applications (Tonina and Jorde, 2013; Passalacqua et al., 2015; Wheaton et al., 2015). Such procedures inherently make use of the details of topographic variability but generally do not analyze or explain variability in and of itself to contextualize observations of Earth surface processes.

Four broad approaches to characterizing variability are available, but differ in their ability to reveal underlying geomorphic mechanisms shaping landscapes – classic statistical description (Scown et al., 2015), classic time series analysis (Kumar and Foufoula-Georgiou, 1997; Furbish, 1998; Parker and Izumi, 2000), geostatistics (Legleiter, 2014), and object-oriented analysis (Hay et al., 2001; Halwas and Church, 2002). This study employs geomorphic covariance structure (GCS) analysis (originating in Brown and Pasternack, 2014, 2017), a blending of time series, object-oriented, and geostatistical approaches, to investigate patterns of morphological variability that constitute the topographic regime of a canyon-confined mountain river. GCS analysis also indicates how variability patterns drive fluvial geomorphic processes responsible for nested longitudinal sequencing of fluvial landforms. The introduction summarizes terminology and concepts necessary to understand GCS analysis, including how this approach can help guide interpretations of hydro-morphodynamics.

Background terminology

The terms “scale”, “scale independent”, and “nested” are widely used in geomorphology, but are rarely carefully defined or used consistently. The term “scale” is often used in geomorphic articles to refer to a particular size of something (i.e., its domain), whether in time or space. For example, many studies characterize fluvial landscapes as consisting of spatial domains of decreasing size, such as catchments, reaches, and geomorphic units (e.g., Frissell et al., 1986; Thomson et al., 2001). In this study using GCS analysis, “scale” similarly refers to a particular spatial domain of geomorphic significance. However, most past studies do not pay attention to the centering/positioning of a smaller scale relative to a larger scale. In GCS analysis, scale adheres to the same spatial domain concept, but it differs in that the extent of all scales are centered on the river corridor and are fixed to the same corridor length. The lateral extent of each scale is dictated by the hydro-morphological condition of discharges with different magnitudes, as indicated by water surface elevation (i.e., “stage”). For example, the base flow channel, bankfull channel, floodprone area (i.e., corridor width at double bankfull depth), and onset of valley walls are all individual spatial scales for which the longitudinal domain is held fixed, but each has a different lateral extent corresponding to the width inundated by the water surface elevation that just fills the channel extent given the shape of the topography. Holding the length fixed is key to understanding how these different scales work together to produce the entirety of the (natural) topographic regime, which is done through analysis of nesting (a term to be defined shortly).

The term “scale independent” means that the object or variable of interest has no inherent dimensional size. For example, the objects “particle” and “bowl” cannot be said to be absolutely 0.01 or 100 m measured along the longest axis. Their size is unknowable from the term alone. In geomorphology, some objects do have fixed dimensions by convention, such as “gravel” (Wentworth, 1922), but purely geometric objects (e.g., “nose”, “saddle” and “nozzle”) are scale independent. The term scale independent may apply to not only a single object with one definitive shape, but several simple objects connected together (e.g., a hillslope nose connected to a hollow) or a single object with many surficial geometric variations.

The term “nested” means that the topographic structure at any smaller scale is literally inside of that at a larger scale (Figure 1a), which necessitates that structures are discernable, separable, and additive (e.g., through signal processing analysis). Building on scale independence, imagine placing a small bowl inside a medium bowl inside a large bowl. The geometric archetype of a bowl is scale independent, and it can be assigned to multiple scales fixed at the same location – all three bowls have the same center, but then extend away from that center to varying distances. This is the same concept as in the traditional geomorphic meaning of nested, but herein applied to the specific set of scale independent fluvial landform archetypes delineated in the GCS framework.

Given this terminology, the topographic regime of a mountain river corridor can be interrogated. As these introductory concepts are developed below, the example of a dryland, partially confined alluvial river corridor (Figure 1b) is used to illustrate them.

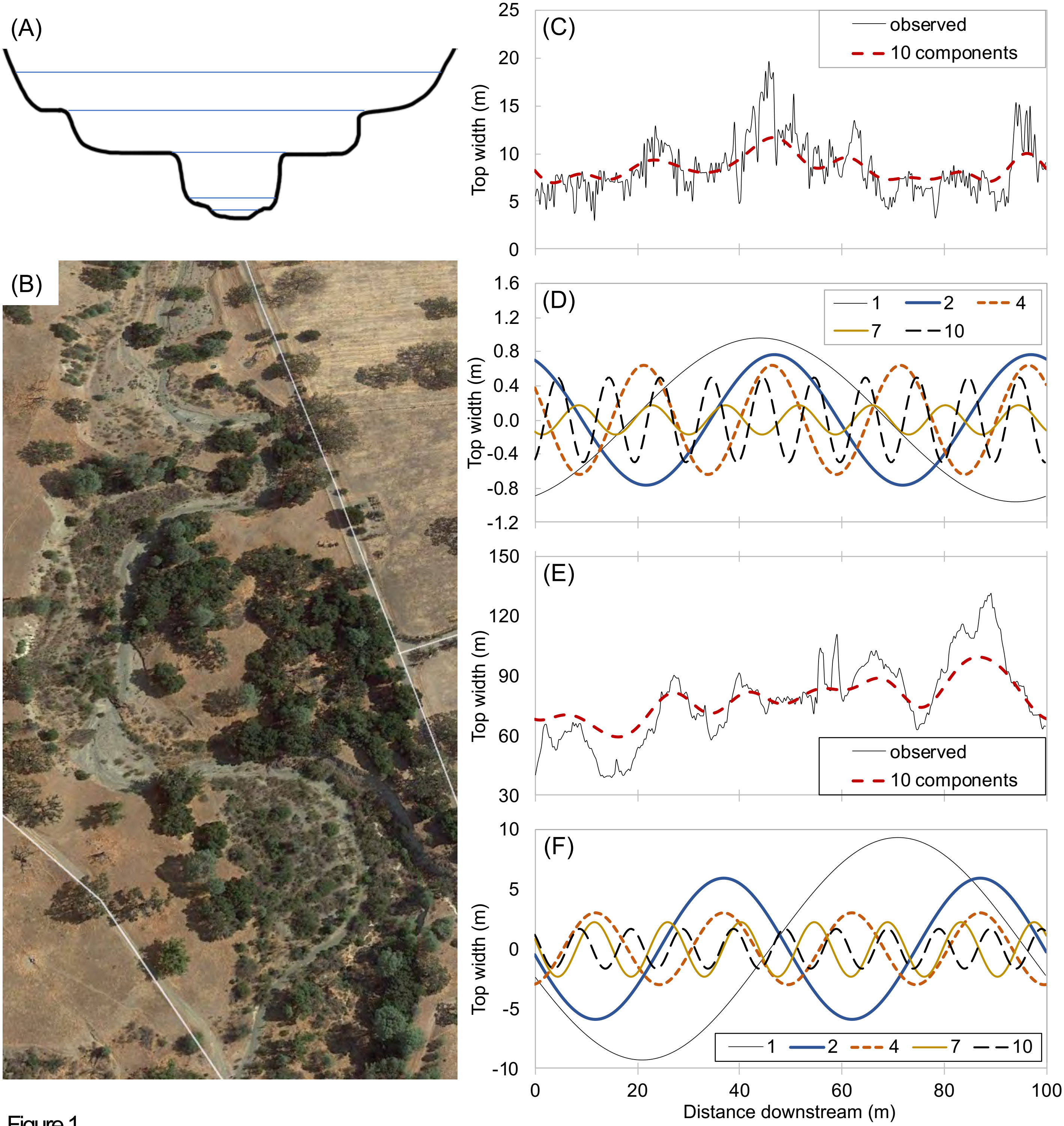
(A)
(B)
(C)
observed
10 components
Top width (m)
(D)
1
2
4
7
10
Top width (m)
(E)
observed
10 components
Top width (m)
(F)
1
2
4
7
10
Top width (m)
Distance downstream (m)

Figure 1

This example with no water visually portrays multiple nested spatial scales of channels carved inside a river corridor, such as conceptualized in Figure 1a.

Fluvial spatial series

Many measurable variables in geomorphology and allied sciences vary along a pathway, such as down a river corridor. These variables could include sediment attributes, topographic changes, biotic variables, flow-dependent hydraulics, and flow-independent measures of topography (e.g., Moody and Troutman, 2002; Brown and Pasternack, 2014). Longitudinal variations in river morphology, such as in river width and depth, can contain stochasticity and chaotic nonperiodic fluctuations, but to a large degree are highly organized and interrelated (Brown and Pasternack, 2017; Palucis and Lamb, 2017; Pasternack et al., 2018a,b) owing to their lability and tendency for mutual adjustment to external forcing (Hack, 1960).

Mathematically, the longitudinal profile of any variable along a reach, such as channel width, can be extracted at equal increments for any scale fixed on the river corridor (Figure 1c,e) and then decomposed into its constituent additive, continuous elements (Figure 1d,f), each with an absolute amplitude, frequency, and phase – or similar parameter for other methods of series decomposition, such as Fourier or wavelet analysis. Typically, a small-scale geomorphic spatial series will have higher frequency, lower amplitude, statistically significant fluctuations reflecting topographic control of landforms existing at the next few higher spatial scales. A large-scale geomorphic spatial series will have lower frequency, higher amplitude, statistically significant fluctuations, reflecting mountain-valley scale topographic controls. Alternatively, an object-oriented approach to decomposition can be employed (Wyrick et al., 2014), but as of yet this lacks the same amenability to spatially continuous mathematical representation and procedural generation (Brown and Pasternack, 2019).

River variations at each of several scales can also be nested, like a bowl inside a bowl inside a bowl. This constitutes multiple spatial scales of nested morphological structure. The entirety of these nested spatial patterns is not only quantifiable, but significant for controlling fluvial morphodynamics (Pasternack et al., 2018 a,b). Lane et al. (2017) reported that for a large region of California, river morphology variability metrics (such as the coefficient of variation of width and depth at baseflow and bankfull discharges) distinguished channel types better than traditional central tendency river attributes (e.g., reach-average values of width, depth, channel slope, width-to-depth ratio, confinement, and dominant substrate size). Both geomorphic processes and ecological functions are more strongly governed by the nested scales of spatial variability in river corridor topography than by the central tendency of a river averaged over scales (Frissell et al., 1986; Kieffer, 1989; Thoms, 2006; Sheldon and Thoms, 2006; Warfe et al., 2008). In turn, both geomorphic and ecological processes are vital to maintaining multi-scalar morphological diversity (Gurnell, 1998; Hassan et al., 2008; Wyrick and Pasternack, 2015).

Therefore, a key step in understanding rivers lies in not only quantifying the relations among nested spatial series of any one variable but evaluating how series of different variables relate to each other, as this sets the boundary conditions for the partial differential equations that describe morphodynamics. This defines what we refer to as the fluvial “topographic regime”. Returning to Figure 1, one may wonder how the components of the baseflow corridor shown in panel (c) relate to those in the floodway corridor shown in panel (e). Further, how do both of these width series relate to spatial series of bed elevation, deposition/erosion patterns, large-bed elements, in-stream wood, riparian vegetation, and other biota?

Traditionally, coherency spectral analysis could be used to analyze these relations mathematically (Jenkins and Watts, 1968; Pasternack and Hinnov, 2003), but that technique over-complicates the physical connection between mathematics and geometry, which is critical for geomorphic understanding. The GCS approach provides a means of resolving this dichotomy. Theory and methods about GCS have developed over the last decade but are still emerging. This study uses GCS analysis to gain novel insights about mountain rivers and the morphodynamics that control their landform patterning compared to past approaches.

Geomorphic covariance structure background

Brown and Pasternack (2014) coined the term "geomorphic covariance structure" to mean the linked bivariate pattern of any two river variables along a pathway. GCS is not the same as the statistical covariance, which is a single number. Instead, GCS refers to a different concept involving the complete bivariate spatial series from which a statistical covariance could be computed if desired. The linkage can be a formal mathematical operator such as the product or it can be rule sets, such as a decision tree. The key is to use a link method that reveals underlying processes. A lecture series explaining and applying this theory is available on YouTube (Pasternack, 2020b). Note that GCS analysis is performed on topographic data, which is inherently a snapshot of the river at a moment in time. It may be repeated for each available topographic survey to enable comparisons and evaluate temporal dynamics explicitly.

Geomorphic covariance structures are critical to morphodynamics because they are a significant part of the natural topographic regime that establishes the boundary conditions that dictate how the partial differential equations that govern topographic change dynamics apply to a particular setting. The GCS between detrended standardized bed elevation (Zs), where Zs is a surrogate for depth, and standardized width (Ws) characterizes along-channel changes in cross-sectional area and is the basis for the hydro-morphodynamic mechanism of flow convergence routing (MacWilliams et al., 2006; Pasternack et al., 2018a,b). The GCS between channel centerline curvature and width is relevant for the hydro-morphodynamic mechanism of meander migration via cutbank retreat and point bar growth (Ikeda et al., 1981). A GCS between Ws·Zs and various bed material grain size metrics could be indicative of alluvial step morphodynamics (Curran, 2007) and riffle-pool bed sediment sorting (De Almeida and Rodríguez, 2011). Many other GCSs can be envisioned, opening lines of process-based scientific inquiry that emphasize the role of fluctuating topographic structure.

Geomorphic covariance structures are not only useful for assessing nested topographic patterning of real rivers but also for river designs that more closely mimic natural landforms that drive a diversity of physical processes (Brown et al., 2014, 2015). River Builder software (https://github.com/RiverBuilder/RiverBuilder) uses GCS theory to enable mindful design of multi-scalar fluvial morphological diversity (Pasternack and Zhang, 2020).

Flow convergence routing background

Building on GCS theory, Pasternack et al. (2018a) proposed a continuum-based, scale-independent approach to classifying landforms with respect to a single morphodynamic mechanism that can occur at many fluvial scales. The approach is amenable to signal processing analyses that enable the same typology to be employed over the same wide range of scales spanned by the mechanism itself. This capability provides a unified descriptive framework for fluvial process-morphology linkages for any one process. To make the concept substantive, the morphodynamic mechanism of flow convergence routing (FCR) was chosen as the focus of intensive inquiry (see Pasternack et al. (2018a) for background literature, classification scheme, and data analysis methods), and this study continues that effort in a different setting addressing a different scientific question.

In essence, FCR involves longitudinally varying spatial funneling of flow (i.e., ‘convergence’) by nonuniform topography that is inundated to varying degrees by different flow stages. Locations of most concentrated flow (i.e., geometric constrictions) at any discharge have the highest potential to scour and route sediment through them (Clifford, 1993; MacWilliams et al., 2006; Pasternack et al., 2018a). In contrast, locations of least concentrated flow at any discharge (generally oversized cross-sections) have flow divergence and the highest likelihood of sediment deposition at that flow. Flow convergence relates to the hydraulic aspect of the mechanism and routing relates to its sediment transport dynamics. The FCR morphodynamic phenomena is well-documented in free-formed, low-to-moderate gradient (≤ 1% bed slope), gravel bed rivers (Keller and Florsheim, 1993; Sawyer et al., 2010) as well as in forced-pool channels (Thompson et al., 1999). However, documentation of FCR in canyon-confined mountain rivers is generally lacking (Harrison and Keller, 2007).

The most important aspect of FCR is that this process is capable of yielding freely self-maintaining (sensu Leopold, 1962) landform sequences if river topography has a particular nested structure of alluvial sediment in which constrictions and expansions shift spatially as a function of discharge (Figure 2), all other things being equal (e.g., sediment size, boundary roughness, and bed slope). Specifically, small cross-sections (considering depth and width together) that are subject to high sediment transport capacity at low flow (Figure 2a,c XS1 red arrow) must be nested within large cross-sections that have low sediment transport capacity during overbank flows (Figure 2a,c XS1 orange arrow) for FCR to yield freely self-maintaining landform sequences. These locations may become armored during long durations of low flow, but are renewed by a mixture of coarse sediment sizes during floods. Note that cross-section orientation changes with discharge to remain perpendicular to the wetted area centerline. Conversely, locations with large cross-sections at low flow must become small cross sections (considering depth and width together relative to cross sections upstream and downstream) at high flow (Figure 2a,c XS 2 blue arrows), so that any fine sediment deposition under normal conditions is scoured out and pool dimensions maintained during floods. This type of nesting with stage-dependent cross-sectional area “reversals” driving freely self-maintaining landform sequencing is common in free-forming alluvial rivers with riffle-pool morphology (MacWilliams et al., 2006).

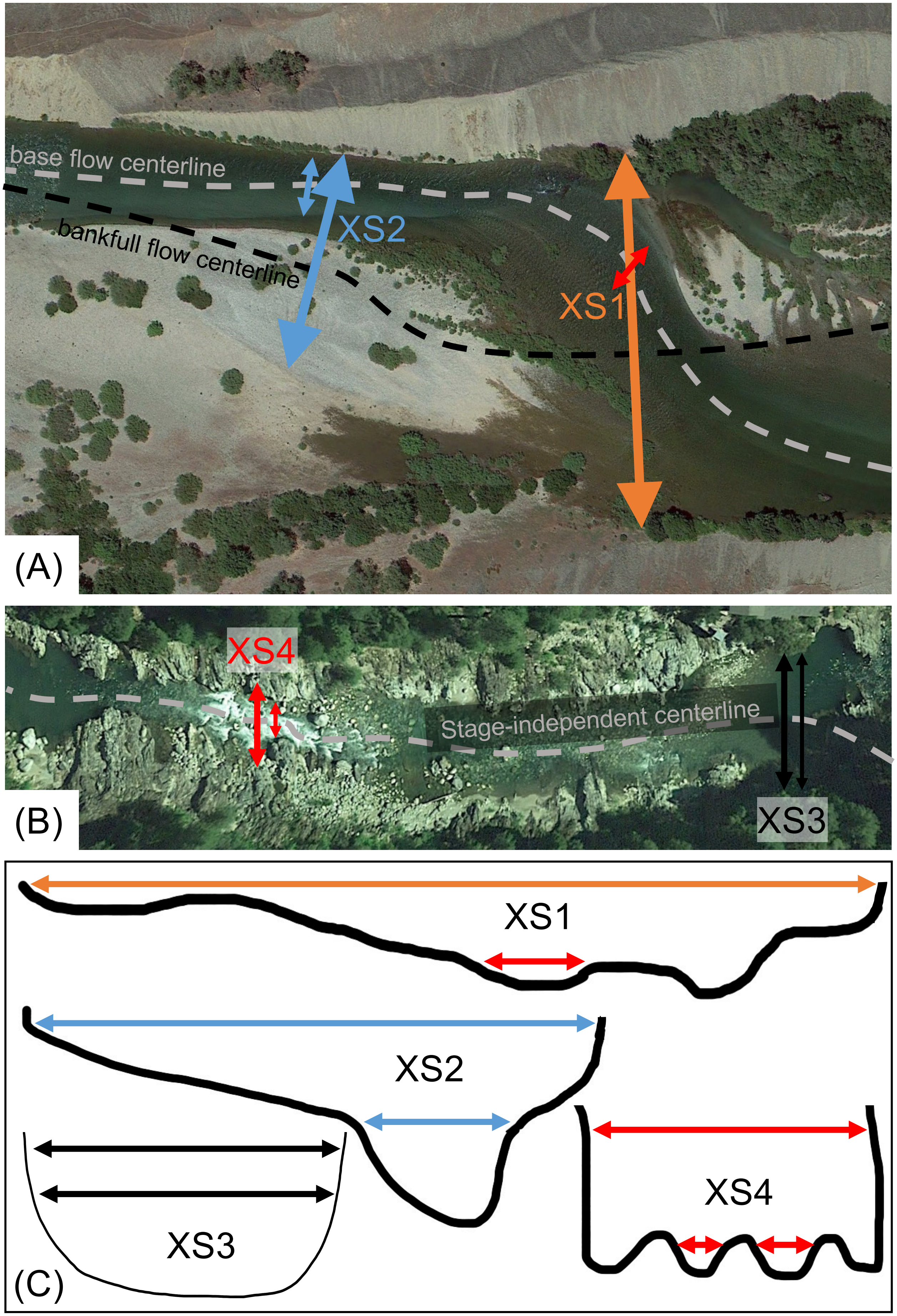
base flow centerline
bankfull flow centerline
XS2
XS1
(A)
XS4
Stage-independent centerline
XS3
(B)
XS1
XS2
XS4
XS3
(C)

The opposite nesting scenario that is not freely self-maintaining is bountiful in nature, but it must be forced by virtually unmovable oversized coarse sediment, wood jams, bedrock, or human-built structures to avoid losing topographic diversity. In this scenario, some locations always have the lowest cross-sectional area and are thus always the focus of scour (Figure 2b,c XS4 red arrows). Conversely, fixed locations with the largest cross-sectional areas are always the focus of deposition (Figure 2b,c XS 3 black arrows), yet rarely fill in due to low sediment supply. In alluvial rivers whose flood regime is sufficient to move the bed material when discharge is sufficiently high, this topographic regime cannot persist given adequate sediment supply, because small cross-sections will scour and large cross-sections aggrade until all locations equilibrate at roughly average dimensions. However, mountain ranges have extensive corridors with low sediment supply and fixed forcing elements resistant to erosion that can maintain this nesting structure (Montgomery et al., 1995). Note that it is possible that apparently non-self-maintaining, forced landform sequences (when focusing on the smaller nested scales in a corridor) could actually be freely self-maintaining if sufficiently high flood discharge occurs and is capable of freely re-arranging forcing elements by causing a cross-sectional area reversal per the mechanism described above. The conjecture in the previous sentence is the topic of this study.

Prior to GCS analysis, FCR characterization required hydrodynamic modeling (e.g., Jackson et al., 2015; Strom et al., 2016) and extensive expert-based interpretation. Numerical modeling is highly effective and more spatially precise but requires substantial effort (especially when scaling up to long river networks). Modeling is also far more difficult to automate than GCS analysis of a DEM, because it has many data input and parameter selection requirements, not to mention an expectation of model validation (Pasternack, 2011). GCS can take immediate advantage of the growing availability of topo-bathymetric DEMs for rivers lacking extensive stage and discharge gages, while numerical modeling cannot.

According to FCR theory, a diagnostic connection exists between detrended bed elevation and wetted width at each flow stage that can be used to reasonably assess FCR without numerical modeling. Specifically, all other things being equal, at discharges with a sediment transport capacity sufficient to drive erosion and deposition in response to nonuniform topography, FCR dictates that freely self-maintaining landform sequences have cross sections with a positive correlation between Zs and Ws as well as a positive value for the product Zs·Ws (Brown and Pasternack, 2014; Brown et al., 2014, 2015; Pasternack et al., 2018a,b). The cited articles explain how these GCS metric values indicate a sequence of wide riffles and constricted pools, whose requirements for self-maintainability have been thoroughly researched for decades (see literature review by MacWilliams et al., 2006). Conversely, a landform sequence with non-self-maintaining FCR forced by immovable elements exhibits an inverse correlation between Zs and Ws as well as a negative value for the product Zs·Ws.

Building on this simple concept, Pasternack et al. (2018b) laid out a thorough, transparent, standardized, analytical framework that guides geomorphologists in their use of GCS methods to assess FCR in any river (Table 1). The framework addresses four high-level study objectives, each having three to five specific, tractable scientific questions (14 total) applicable to all rivers. To be clear, Table 1 is reproduced here as background; the questions in Table 1 were all answered in this study as part of the

Table 1. Geomorphic covariance structure analysis framework applicable to any river.

Objectives (O#) and their questions	Test variables	Analysis
(O1) Analyze stage-dependent structure of fluvial topographic deviation from central tendency using longitudinal series of standardized width (Ws) and detrended, standardized bed elevation (Zs) for multiple flow stages.		
(1a) What percent of the river has topographic variations greater than 0.5 and one standard deviations away from the mean?	Abs(Zs), Abs(Ws)	percent of values > 1 or > 0.5
(1b) Is longitudinal topographic structure random?	series of Zs, Ws	Wald-Wolfowitz* runs tests
(1c) Are width and bed elevation series correlated, as one indicator of coherent organization?	series of Zs, Ws	Pearson's product-moment correlation for Ws and Zs
(O2) Analysis of presence of flow convergence routing using Ws·Zs spatial series for multiple flow stages.		
(2a) At what stage and discharge, if any, does the morphological structure abruptly change from negative to positive covariance?	series of Ws·Zs	mean(Ws·Zs); percent of values > 0
(2b) What stage and discharge ranges, if any, exhibit self-sustainable morphology consistent with a dominant role for flow convergence routing?	series of Ws·Zs	mean(Ws·Zs); percent of values > 0
(O3) Analyze relative abundance and longitudinal sequencing of landforms by reach and discharge.		
(3a) What is the relative abundance of each landform for the whole river for each flow?	series of landform IDs	count and compare
(3b) How do geomorphic reaches compare in landform composition?	series of landform IDs	count and compare
(3c) How does landform abundance change with flow?	series of landform IDs	count and compare
(3d) What is the longitudinal sequencing of landforms?	series of landform IDs	count times each unit followed another
(3e) How does longitudinal sequencing change with flow?	series of landform IDs	count times each unit followed another
(O4) What is the stage-dependent, nested structure of landforms classified by their flow convergence routing potential?		
(4a) What are top five most abundant nested permutations?	nested series of landform IDs	permutation abundance analysis
(4b) For each landform at the floodprone scale, what are the top three most abundance nested permutations?	nested series of landform IDs	permutation abundance analysis
(4c) For each bankfull scale landform, what are the top two most abundant nested permutations of base flow landforms?	nested series of landform IDs	permutation abundance analysis
(4d) For each landform at the bankfull scale, what are the top two most abundant floodprone landform hosts?	nested series of landform IDs	permutation abundance analysis

*Wald and Wolfowitz (1940)

steps of working through the GCS procedure, but are not the study purpose for this article, in and of themselves. As explained in detail in the next section, this study asks a specific question about a specific type of river by drawing on the results generated from answering the 14 GCS scientific questions listed in Table 1 from prior research. This study has its own additional experimental design (not Table 1) described in the experimental design subsection of the methods section. Explaining the theory and basis for the GCS framework is beyond the scope of this article and the interested reader is referred to Pasternack et al. (2018a,b).

Study purpose

Prior approaches to studying mountain river morphodynamics rely on sediment mobilization prediction with no capability to explicitly address landform self-organization. Mountain rivers typically have a mixture of coarse sediment, including framework boulders structurally supporting a landform (Zimmerman and Church, 2001; Curran, 2007). Consequently, there exist low discharges wherein bed material is predominantly stationary. Traditionally, empirical equations reliant on overly simple hydraulics with consequential, questionable assumptions are employed by geomorphologists to roughly estimate the discharges required to move these framework boulders (e.g., Grant et al., 1990; Zimmerman and Church, 2001). These flows are then often assumed to be the ones initiating and controlling landform patterning and its re-organization. Alternately, 1D hydrodynamic modeling has been used to yield improved estimates accounting for backwater effects in gradually varying flows (e.g., Baker and Pickup, 1987), assuming cross-sections are available at all hydraulic controls and ignoring rapidly varying flows.

Today, 2D hydrodynamic modeling is used for mountain flood modeling and bed shear stress estimation, and this tool is most effective where digital elevation models are available (e.g., Pasternack and Senter, 2011).

However, all of these approaches rely on the same, classic assumption that sediment entrainment (as indicated by estimated bed shear stress) drives landform re-organization (e.g., Baker and Ritter, 1975), with no coherent geomorphic processes at work (e.g., knickpoint migration, flow convergence routing, alluvial step formation, etc.). Threshold discharges for entrainment identified by sediment transport methods are assumed to be the ones initiating and controlling landform patterning and re-organization without strong evidence to support this assumption. The relative roles in landform re-organization of any discharges higher than those initiating sediment transport cannot be investigated by this method, because there are no known linkages between specific Shields stress thresholds and different stages or types of landform re-organization for coarse-bedded mountain rivers. Meanwhile, important migratory channel processes that re-organize mountain river landforms, such as knickpoint migration, step dynamics (Curran, 2007) and sequentially triggered landform failure processes (Pasternack et al., 2008) cannot be inferred by this method and yet play an important role in mountain rivers. How then does one identify and account for such processes?

This study goes beyond the questions in Table 1 by introducing a different scientific application of GCS analysis that addresses the problem explained in the preceding paragraph without calculating shear stress. Specifically, it employs GCS analysis and the results from answering the questions in Table 1 as a diagnostic tool to ascertain the flow stage, if any, at which mountain rivers switch from exhibiting forced hydraulics over immovable terrain with little FCR morphodynamics to free hydraulics over adjustable terrain with appreciable FCR morphodynamics. In this context, “free” means that the river’s dynamism yields a self-organized interplay between topography-driven forced hydraulics and hydraulics-driven topographic change.

The scientific hypothesis evaluated in this study is that fixed, non-self-maintaining landforms at a smaller scale are nested inside freely self-maintaining landforms at a larger scale. The underlying conceptualization of a stage-dependent morphodynamic mechanism for mountain rivers remains the same as in past literature, but the target of inquiry shifts from looking for the onset of sediment transport with increasing stage to the onset of freely self-maintaining FCR landform structure within increasing stage. Table 1 does not specify a question to find such a threshold, because it was not asked in the prior research, but it does provide the data to answer the question and test the hypothesis in the first sentence of this paragraph, further emphasizing that the questions in Table 1 are not the study purpose.

Previous studies used GCS analysis to argue that gravel/cobble river landforms at a spatial scale of 1-2 times bankfull stage had the most coherent longitudinal landform sequencing consistent with FCR morphodynamic control (Brown and Pasternack, 2017; Pasternack et al., 2018b). In those cases, however, rivers had freely self-maintaining FCR landform sequences at all stages due to their smaller grain size, lower valley positioning, and high-amplitude width undulations across nested spatial scales. This study considers more mountainous environments to see if coarser confined rivers with extensive bedrock outcropping and large boulders only moved by very large floods ever reach a flow high enough to transition from non-self-maintaining to self-maintaining FCR landform sequencing. If so, then this study provides a means of estimating the stage and discharge at which this shift occurs. In this approach, it is not necessary to directly observe, estimate, or predict sediment entrainment or initiation of geomorphic processes. Instead, the structure of landform sequencing and nesting is queried for tell-tale indicators of freely self-maintaining FCR landform organization.

Study area

Geographic setting

The Yuba catchment in California drains ~ 3480 km^2 of dry summer subtropical mountains to the confluence with the Feather River (Figure 3). In the Sierra Mountains the Yuba River has three major subbasins: North Yuba (1,271 km^2), Middle Yuba (544 km^2), and South Yuba (912 km^2). Like many mountain regions, this one underwent cumulative anthropogenic impacts, including hydraulic gold mining (Gilbert, 1917; James, 2005), timber harvesting, land use, and flow regulation. While the Middle Yuba River has a few small reservoirs, the North Yuba River has multi-purpose New Bullards Bar Reservoir, California's 2nd tallest dam (5th tallest in the United States) and 13th largest water storage capacity. This dam is a complete barrier to bedload transport and has a very high trapping efficiency for suspended sediment, with the exception of some fine-grained wash load.

The study segment includes the ~ 3.5 km reach of the North Yuba below New Bullards Bar Dam and another ~ 9.7 km portion of the mainstem Yuba River from the

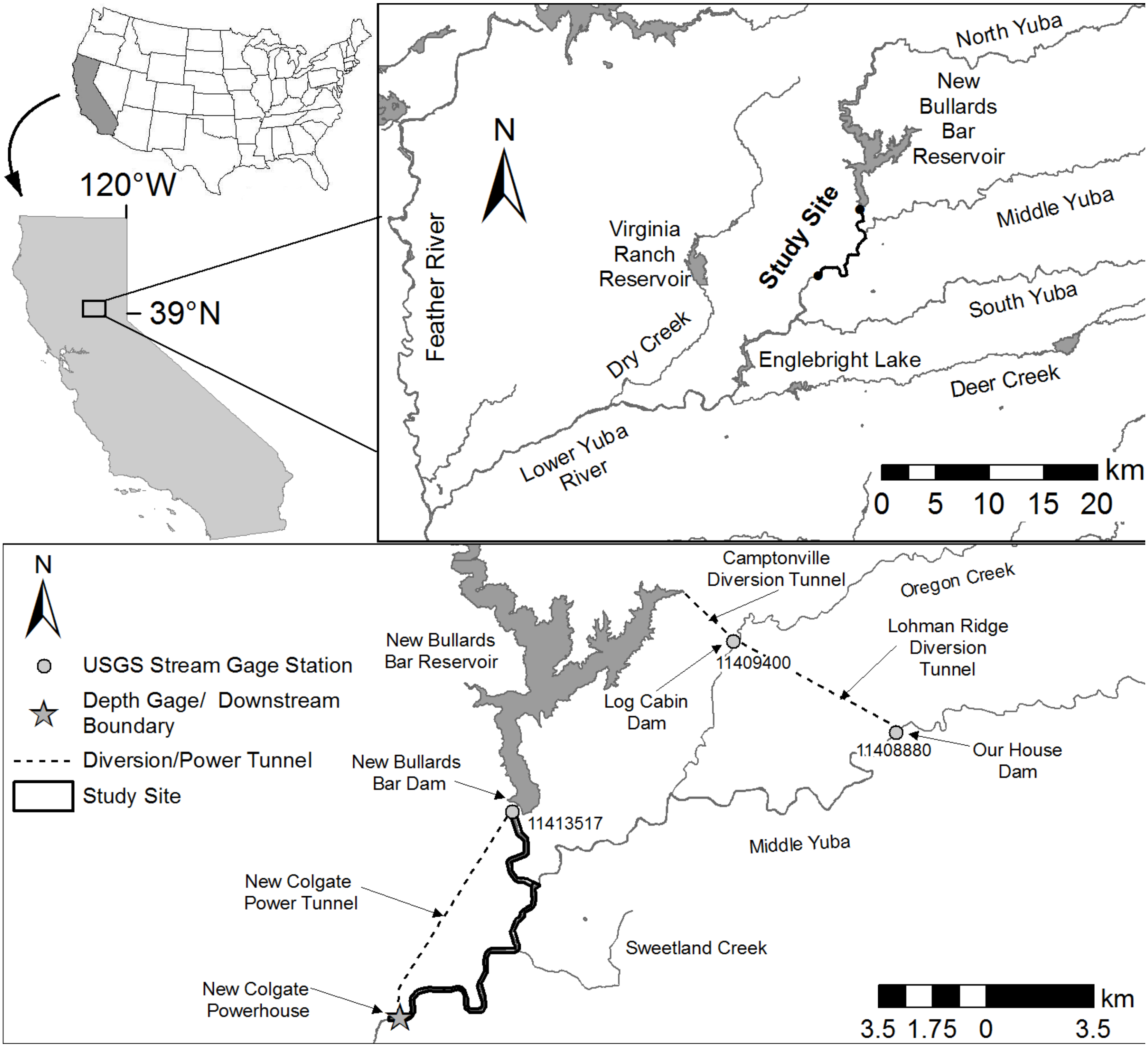
120°W
39°N
N
North Yuba
New Bullards Bar Reservoir
Middle Yuba
Study Site
Virginia Ranch Reservoir
Feather River
South Yuba
Dry Creek
Englebright Lake
Deer Creek
Lower Yuba River
km
0 5 10 15 20
N
USGS Stream Gage Station
Depth Gage/ Downstream Boundary
Diversion/Power Tunnel
Study Site
Camptonville Diversion Tunnel
Oregon Creek
New Bullards Bar Reservoir
11409400
Lohman Ridge Diversion Tunnel
Log Cabin Dam
11408880
Our House Dam
New Bullards Bar Dam
11413517
Middle Yuba
New Colgate Power Tunnel
Sweetland Creek
New Colgate Powerhouse
km
3.5 1.75 0 3.5

Figure 3

confluence of the North Yuba and Middle Yuba to just upstream of New Colgate Powerhouse. The segment is a complex, low sinuosity, boulder-bedded, 5th-order mountain river confined within a steep-walled bedrock and forested hillside canyon. The overall mean bed slope is 2% varies locally with some sites exhibiting slopes >10%. Based on limited sedimentological data (Curtis et al., 2005; James, 2005; YCWA, 2013) bed substrates alternate between bedrock and alluvial sections with estimates of larger boulders (>512mm) or bedrock covering ~ 65% of the study segment. Sediment storage capacity within the study segment contrasts between sections, with bedrock sections lacking large storage capacity and the limited alluvium present commonly being restricted to deep pools or zones of low velocity or recirculating flow in the wake of large boulders and bedrock outcrops (Curtis et al., 2005). Alluvial sections have sediment storage capacity in the channel bed and along intermittent bars (Curtis et al., 2005; James, 2005). Regardless of location, alluvial substrate present is a heterogeneous mixture of materials dominated by coarse fractions (medium gravel/cobbles and larger clasts). The presence of large boulders and the heterogeneity of sizes makes grain size quantification difficult and labor intensive, if attempted at all.

The near continuous presence of the valley margin, defined as the contact between the predominantly alluvial valley floor and bedrock hillslope (sometimes with a thin soil mantle), along both banks results in a bedrock confined valley setting (*sensu* Fryirs et al., 2016). The high degree of confinement strongly influences the ability for lateral channel migration, often dictating the character and behavior of a river as well as the suite of geomorphic landforms present (Brierley and Fryirs, 2005; Wheaton et al., 2015). Similar to other bedrock-confined rivers, the study site lacks a contiguous floodplain and includes only localized floodplain pockets at major tributary junctions, meander bends, or other areas of local valley widening (Fryirs et al., 2016).

Hydrologic Setting

Detailed Yuba catchment hydrologic information is readily available (YCWA, 2012; Wiener and Pasternack, 2016a). Presently, water resources in the vicinity of the study segment are heavily regulated for flood protection, power generation, and water management. Flows into the study segment are the combined input of releases from New Bullards Bar dam and Middle Yuba flows as well as flow accretion from groundwater and overland runoff. Flow records below the dam are available from United States Geological Survey gaging stations 11413517 and 11413520. Based on data from these stations for the period August 1966 – February 2016 (18,097 days) the median and 90th percentile mean daily releases below the dam are 0.18 and 0.37 m^3/s, respectively. Occasional large storms require larger releases. Over this period mean daily flow was recorded as exceeding the capacity of the dam’s low flow release (35.40 m^3/s) on 713 occasions. Regardless of these large events most of the discharge and sediment input to the study segment is supplied by the Middle Yuba River.

The Middle Yuba River has a complex system of small dams and diversions for water resources management. The two downstream channels that supply the study segment are the Middle Yuba River below Our House Dam and Oregon Creek below Log Cabin Dam. Their flow records (stations 11408880 and 11409400, respectively) show that the combined median and 90th percentile mean daily flows for the period

October 1968 – February 2016 are 1.30 and 3.52 m^3/s, respectively. The peak discharge for the study segment estimated over the period of record was 2161 m^3/s.

Methods

Experimental design

Does a mountain river exhibit a threshold shift in landform structure from fixed non-self-maintaining landforms at low stage to freely self-maintaining landforms at high stage? This specific, new scientific question was answered herein with a transparent experimental design consisting of eight tests extracted from and building on the overall GCS framework (Table 2). Data came from 2944 cross-sections spaced equally (4.572 m, 15 ft) along the 13.2-km Yuba River study segment. The first two columns of Table 2 list a specific GCS question from Table 1 and the values of the GCS metrics required to corroborate the hypothesis explicitly stated in the study purpose section of this article. The third and fourth columns of Table 2 present study results and conclusions, respectively, so the entire experimental design and outcome is accessible in a single table. Table 2 is different from Table 1 not only in that it uses a subset of Table 1 questions and results, but also in that it compares and contrasts GCS metrics for low versus high discharges to seek a possible threshold change. Prior research that developed and applied Table 1 never did that.

In general, Ws versus Zs correlations and Ws·Zs metrics indicate the capacity for freely self-maintaining landform sequences with a connection between the magnitude of these metrics and the dominance of FCR as a driving mechanism. Landform

Table 2. Hypothesis testing outcome indicators and results.

Table 1 ID	Values required to corroborate hypothesis* low stage	high stage	threshold Zd**	corroboration?
1c	negative correlation	positive correlation	4.6-7	Y
2a	negative mean Ws·Zs	positive mean Ws·Zs	4.6-7	Y
2a	< 50% XS have Ws·Zs > 0	> 50% XS have Ws·Zs > 0	4.6-7	Y
3c	more O than CP	more CP than O	2-4.6	Y
3c	more NZ than WB	more WB than NZ	9-13	Y
3d	O-NZ sequences	CP-WB sequences		N
	landform nesting expectation			
4c	baseflow WB and NZ nested within bankfull WB		n/a	mostly
4c	baseflow O and CP nested within bankfull CP		n/a	mostly

*XS means cross-section, O=oversized, CP=constricted pool, NC=normal channel, WB=wide bar, NZ=nozzle. Geometric shape delineation method presented later in the text.

sequencing and nesting metrics reflect the local-scale topographic regime in terms of pairing of adjacent or nested landforms and indicate the degree to which the landforms might be a manifestation of functional FCR at different scales.

Six tests have test-metric requirements at both low and high stages for the hypothesis to be corroborated or rejected. For these tests a yes or no outcome exists as to whether a threshold is present or not. If no threshold is present, then two scenarios could be involved: either landform sequences are freely self-maintaining at all stages or none are, or at least not in the range of discharges investigated.

The last two tests involve examination of landform nesting, seeking a specific nesting structure (Table 2). While an expected nesting structure for freely self-maintaining landform organization exists (see FCR background presented above), no known percent threshold exists for how many nesting cross-sections along a river corridor must meet this expectation. Other geomorphic processes operate concurrently with FCR and could drive alternative landform structure. Therefore, these two tests are assessed for the relative abundance of the expected nesting structure but are not interpreted strictly as would be required to corroborate the hypothesis. A better understanding of nesting metrics will emerge when more rivers are investigated with this framework.

Corroboration of the hypothesis as a whole does not require the same threshold stage value for all metrics, because different reaches and local landform sequences may have different FCR morphodynamics. Some tests might corroborate the hypothesis and some might refute it, which would suggest a complex assemblage of processes governing the river instead of a dominance of FCR morphodynamics. Instead of trying to force an arbitrary quantitative criterion for overall corroboration, test results are transparently presented and discussed.

Data collection and processing

This study focused on evaluating four stage-dependent spatial series (Zs, Ws, the product Ws·Zs, and landform identification codes) at seven stages. To obtain these spatial series, this study introduced a procedure for characterizing and interpreting river morphology with nothing but a meter-scale DEM (Figure 4).

A DEM of the study segment was produced from four data inputs collected during a drought-enhanced base flow in autumn 2014: near-infrared airborne LiDAR, green airborne LiDAR, kayak-based single-beam echo-sounding with real-time kinematic GPS, and color aerial imagery. The last was used with a locally derived depth-versus-color calibration equation to map remote pools deeper than green LiDAR could penetrate and inaccessible for echo-sounding (Legleiter et al., 2004, 2009). A point-cloud-processing procedure was developed and applied that effectively retained extensive natural bedrock and boulder topographic variability. Wiener and Pasternack (2016b) provide details about this procedure and depth-versus-color calibration approaches/limitations to resolving deep pools. The final point cloud with ~ 70 million points (13.9 pts/m^2) was converted to a 1-m gridded DEM, as sub-meter horizontal variability was not relevant for this study.

Pasternack et al. (2018a) introduced a procedure for stage-dependent Zs and Ws GCS analysis. The procedure not only evaluates longitudinal topographic structure but employs a decision tree to produce a scale-independent landform classification

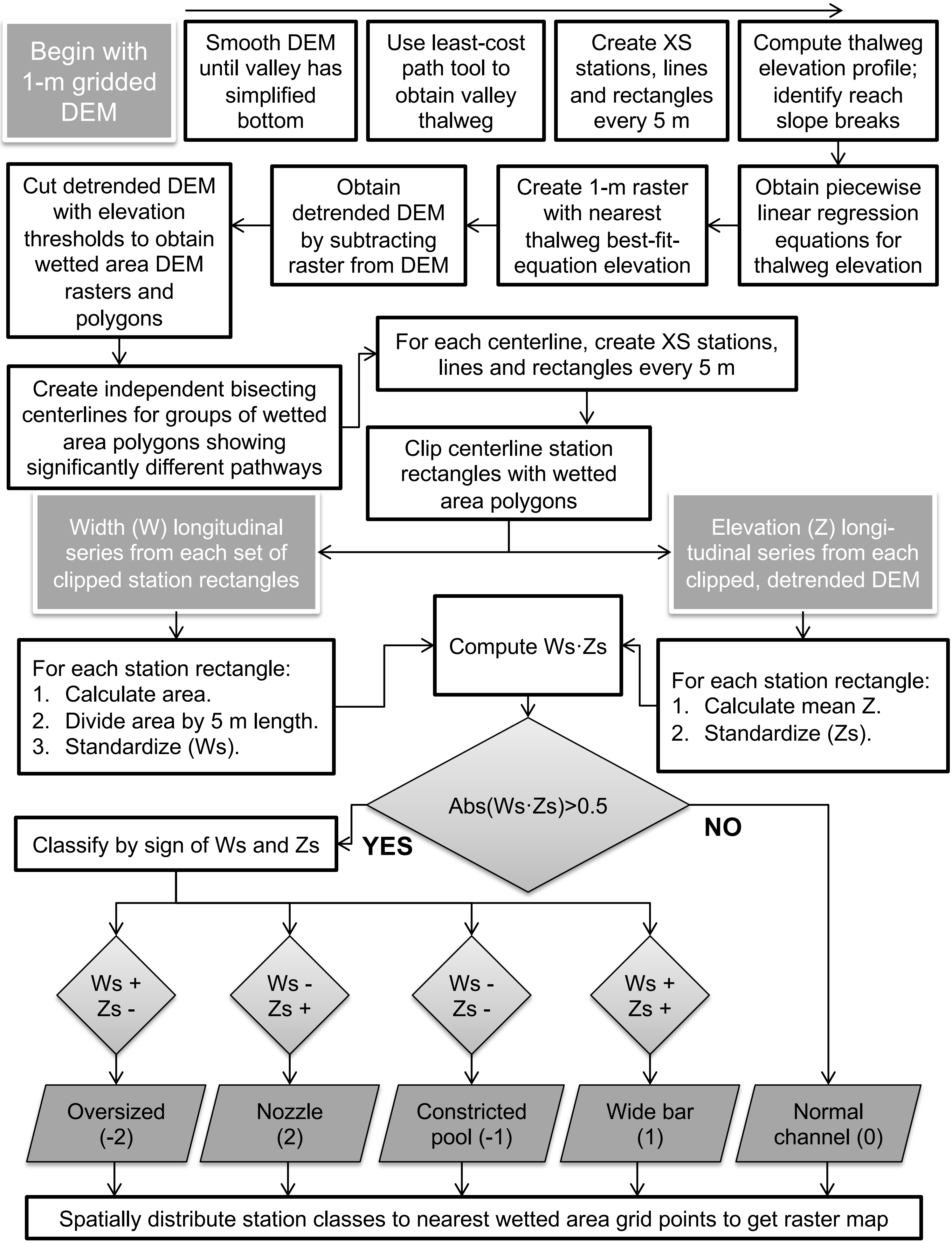

Begin with 1-m gridded DEM
Smooth DEM until valley has simplified bottom
Use least-cost path tool to obtain valley thalweg
Create XS stations, lines and rectangles every 5 m
Compute thalweg elevation profile; identify reach slope breaks
Obtain piecewise linear regression equations for thalweg elevation
Create 1-m raster with nearest thalweg best-fit-equation elevation
Obtain detrended DEM by subtracting raster from DEM
Cut detrended DEM with elevation thresholds to obtain wetted area DEM rasters and polygons
Create independent bisecting centerlines for groups of wetted area polygons showing significantly different pathways
For each centerline, create XS stations, lines and rectangles every 5 m
Clip centerline station rectangles with wetted area polygons
Width (W) longitudinal series from each set of clipped station rectangles
Elevation (Z) longi-tudinal series from each clipped, detrended DEM
For each station rectangle:
1. Calculate area.
2. Divide area by 5 m length.
3. Standardize (Ws).
Compute Ws·Zs
For each station rectangle:
1. Calculate mean Z.
2. Standardize (Zs).
Abs(Ws·Zs)>0.5
YES
NO
Classify by sign of Ws and Zs
Ws + Zs -
Ws - Zs +
Ws - Zs -
Ws + Zs +
Oversized (-2)
Nozzle (2)
Constricted pool (-1)
Wide bar (1)
Normal channel (0)
Spatially distribute station classes to nearest wetted area grid points to get raster map

indicative of FCR morphodynamics applied to each scale. The five landforms are nozzle (NZ), wide bar (WB), normal channel (NC), constricted pool (CP), and oversized (O). That procedure made limited use of 2D hydrodynamic modeling to obtain wetted area polygons (aka inundation zones) and the unique inundation centerline for each discharge, though it mentioned the possibility of obtaining such polygons with no modeling.

This study presents a procedure applicable to all rivers to achieve the envisioned hydraulic-model-free analysis (Figure 4), which saves time and reduces input data needs, though at the cost of some reduction in accuracy. The first part of the procedure (i.e., first two rows of Figure 4) is the same as outlined by Pasternack et al. (2018a), which is to obtain a detrended river corridor DEM. Next, the detrended DEM is now conceptually inundated with water using horizontal planes of incrementally higher detrended elevation to obtain wetted area polygons delineating where a horizontal plane intersects the detrended DEM.

In this study, wetted area polygons for seven discharges were made by specifying a detrended elevation (Zd) value as a water surface elevation (referred to as a "Zd stage") and subtracting the detrended DEM from a raster containing the specified Zd stage value in every cell. Negative values are deleted from the resulting raster as they represent dry areas. Remaining positive values represent depths. The positive-value raster is converted into a single wetted area polygon used to clip rectangles stationed 5 m (in this case) along either a centerline bisecting a wetted area polygon or the least-cost path (i.e., thalweg) down the river to obtain a series of wetted area rectangles (aka stations) for each Zd stage investigated. Wyrick and Pasternack (2014) introduced and explained the cross-section rectangle analysis method. Because this study investigated a confined mountain river (Figure 2b), wetted area polygon centerlines did not vary enough as a function of stage to warrant using a separate centerline for each stage, so the procedure was simplified to use a single centerline for all stages. For partially confined and unconfined river corridors, there tends to be discrete ranges of discharges (e.g., below bankfull, above bankfull but below floodway filling, higher than floodway filling, etc.) over which a single centerline may be used, reducing the need to make a centerline for every flow analyzed. When in doubt, use a unique centerline for each discharge.

The one drawback with this approach to obtaining a wetted area polygon compared to a 2D hydrodynamic model simulation is that it does not account for momentum effects, such as natural backwatering upstream of shallow topographic highs. The consequence is that for low discharges (i.e., low Zd stages) it will cut off those topographic highs and exclude them from the wetted area polygons. This does not occur for flows approaching bankfull and higher, but it does have an impact on base flows. Specifically, where topographic highs are cut off by the water plane, there are no bed elevations or widths available to study, which yields data gaps. This study did analyze two baseflows, but the gaps represent a tiny fraction of the river segment's length.

Inundation zones

No *a priori* set of key Zd stages has been settled on for use in GCS analysis. As GCS becomes further coded as an algorithm in Python, Zd stages could be analyzed for fine increments, enabling careful evaluation of spatial autocorrelation and thresholds. Even then, it is likely that differences in GCS metrics as a function of Zd stage can be captured with just a few stages (Pasternack et al., 2018a), possibly a representative baseflow stage, a bankfull stage (if such a stage is clearly identifiable and scientifically appropriate for a given reach), and a floodway filling stage that might match the definition of the "two times bankfull depth" used in computing a river's entrenchment ratio (Rosgen, 1996). For studies concerned with more extreme floods, a few higher flood stages capable of moving boulders in a confined mountain river would be worth including.

In this study, an expert visual assessment of the detrended DEM was made to identify longitudinally persistent slope breaks indicative of geomorphically carved elevation thresholds that were interpreted to describe different geomorphically relevant inundation zones. Seven different Zd stages were chosen to represent a summer base flow stage, a previously estimated bankfull stage from YCWA (2013), the stage just inundating active gravel bars and approaching the toe of more established bank vegetation (often considered field indicators of bankfull stage), the alluvial bar-to-canyon wall slope break, and three higher flood stages at different slope breaks up the canyon walls. For landform nesting analysis, only three key Zd stages were evaluated, as detailed in the next section.

Because they were not needed for this study, the exact discharge values for these seven Zs water surface elevation values were not investigated thoroughly, but rough flow estimates were made to help interpret results. A limited number of 2D hydrodynamic models were run up to a flow of 343.6 m^3/s on an exploratory basis, with some validation of baseflow depths and velocities (details beyond the scope of this article). Comparison between Zs and 2D model wetted area polygons suggested the best matching discharge. For flows > 343.6 m^3/s, a second-order polynomial was fit through the data points established for the flow range covered by the 2D model and extrapolated to the higher Zd stages. For each estimated discharge, a flood frequency recurrence interval was estimated using United States Geological Survey PeakFQ software (Veilleux et al., 2014). The important point is that the selected Zs range includes floods strong enough to mobilize boulders, destabilize step units, and/or break up armor layers (Grant et al., 1990; Lenzi et al., 2006; Molnar et al., 2010). For example, the largest Zd stage of 17.6 m corresponds to a flow with a 35.9-year recurrence interval, which should yield significant morphodynamics based on videos and field observations of smaller Yuba River floods. Whether such flows would be capable of yielding substantially different landform structure was not known *a priori*.

Upon analysis, wetted area polygons for seven Zd stage values (Figure 5) and their corresponding discharges and recurrence intervals (Table 3) captured geomorphically significant conditions. The Zd stage of 1 m represented baseflow, as it was the lowest stage available and its associated discharge is in the base flow range. A Zd stage value of 2 m is very close to the YCWA (2013) estimated bankfull discharge (10.8 m^3/s). Notably the wetted area polygon for that Zd stage does not inundate the active gravel bar at the confluence with the Middle Yuba River, so it seems low compared to academic bankfull channel delineation expectations. The next higher Zd stage of 4.6 m does achieve that geomorphically significant outcome, and might be a better estimate of bankfull discharge, though it is not important to this study whether it strictly meets that

Table 3. Estimated discharge and flood recurrence interval values for each Zd stage.

Zd (m)	Discharge (m^3/s)	Recurrence interval
1.0	2.7	1
2.0	10.8	1.06
4.6	161	2.4
7.0	350	3.5
9.0	574	6.4
13.0	1171	16.4
17.6	2109	35.9

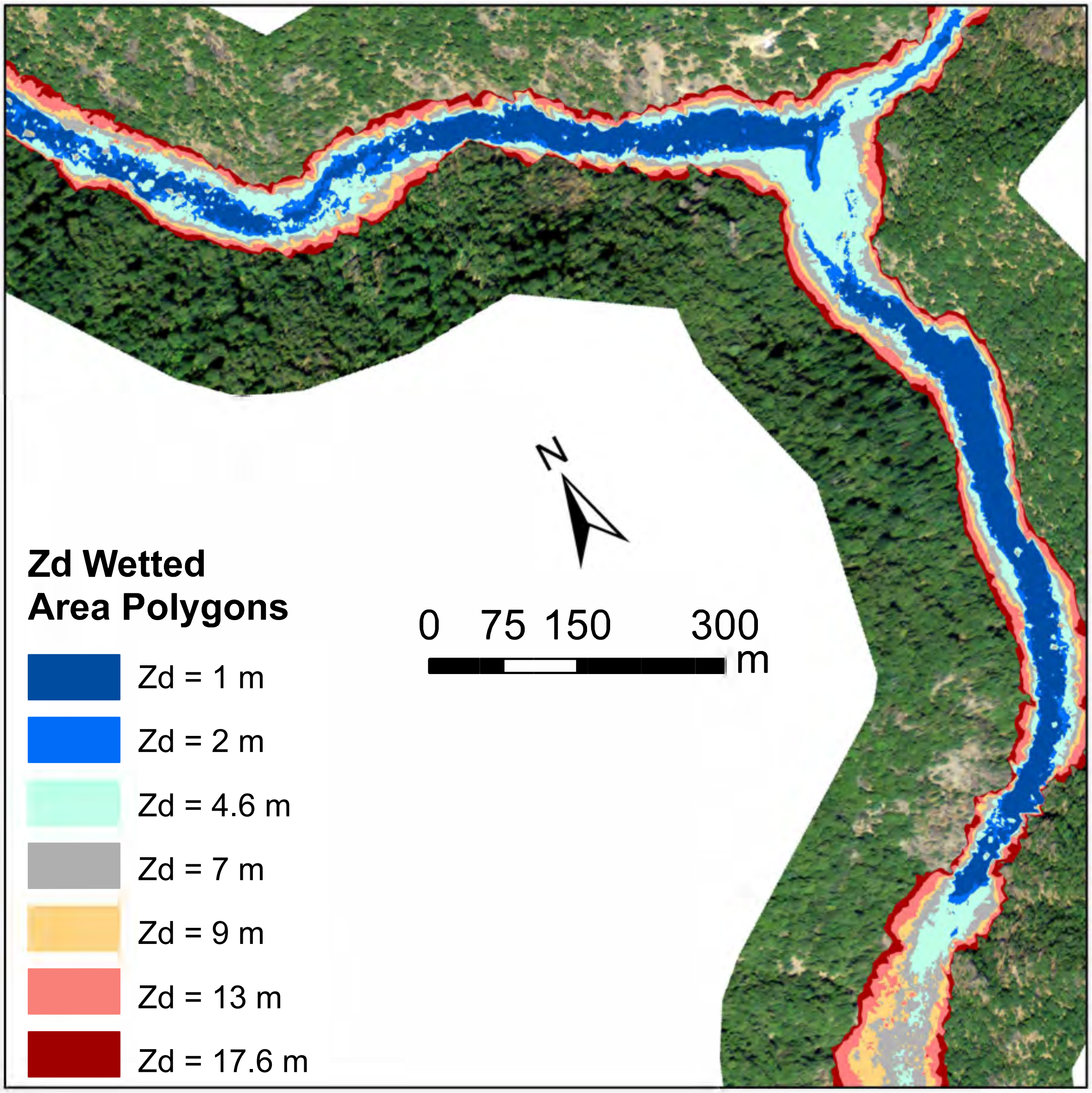
Zd Wetted
Area Polygons
Zd = 1 m
Zd = 2 m
Zd = 4.6 m
Zd = 7 m
Zd = 9 m
Zd = 13 m
Zd = 17.6 m
N
0 75 150 300
m

Figure 5

definition or not. The stage of 4.6 m was also the Zd stage that initiated many stage-dependent transitions in GCS metrics in this study.

By definition (Rosgen, 1996), the floodprone area is the river corridor inundated by a floodprone water stage that yields a riffle thalweg depth that is double reach-average bankfull riffle thalweg depth (assuming riffle-pool channel morphology is present). In GCS analysis using bed elevation detrending, there is no assumption of a riffle-pool or other channel morphology, and thus no pre-delineation of riffles as such to guide determination of a Zd stage strictly following the Rosgen (1996) floodprone stage definition. Instead of referencing to the shallowest landform, Zd stage values are referenced to lateral and longitudinal mean bed elevation. Therefore, a simple, analogous definition of floodprone stage involves doubling the geomorphically identified Zd stage that inundates the active gravel bar. Doubling 4.6 yields 9.2, a value close to the Zd stage of 9.0 m that had been selected independently of bankfull and floodprone flow considerations on the basis of visible lateral slope breaks evident upon inspection of the detrended DEM, so a value of 9.0 was used to represent floodprone flooding.

Data analysis

Data analysis methods to obtain GCS metrics (Table 1) were explained in Pasternack et al. (2018a) to characterize individual variable longitudinal variations, the joint variation of Ws and Zs using the Ws·Zs product function, FCR landform classification, and the sequencing and nesting patterns of FCR landforms. Analyses for objectives 1-3 in Table 1 were implemented for all seven Zd stages, while those for objective four only used three key Zd stages. All analyses were done using ArcGIS®

10.3 for geospatial processing and Microsoft Excel® for statistical analysis. Tests for deviations of standardized values from “normal” (i.e., average) used a threshold value of 1 as a very strict criterion. Once all results were in hand from the methods in Table 1, then the tests specific to this study that are listed in Table 2 were conducted. This involved comparing low and high stage results among seven Zd stages using Microsoft Excel®.

The downstream sequencing of landforms was analyzed to ascertain whether nozzle and oversized units alternate at low stage, while wide bar and constricted pool units alternate at high stage per the ideal sequencing conceptualization for freely self-maintaining FCR morphodynamics (Table 2, test 3d). Across all flows, all units must predominantly transition to normal channel because any time there is a zero-crossing for Zs·Ws, the presence of normal channel is implied by definition. Excluding normal channel from further consideration, the expectation of random organization would be an equal 33% chance of a landform type transitioning to any of the other 3 landform types. To be considered significant for this study, a high threshold of plus or minus 10% was set, meaning that the transition (e.g., nozzle-to-oversized transition) had to occur for > 43% of transition instances or < 23% of transition instances. The proportion of all transitions (as percent occurrences) were tabulated and then visually represented in three ways- a simplified schematic that quickly contrasts results with hypothesis across all stages, color-coded longitudinal profiles of landform types for each stage, and Sankey diagrams for three key Zd stages.

Hierarchical landform nesting (objective 4 in Table 1) was investigated using three out of the seven available Zd stages conceptually representing base flow, the stage just inundating active gravel bars and approaching the toe of more established bank vegetation (often considered field indicators of bankfull stage), and floodprone-area flow for the complexity and permutation reasoning discussed in Pasternack et al., (2018a). With three Zd stages and five landforms, there are 125 available nesting permutations to evaluate how FCR is functioning.

The problem of widely different landform abundances in comparative analysis is usually addressed by normalizing variables with a metric of the relative abundance of each landform (e.g., Wyrick and Pasternack, 2014). For example, if a river has few nozzles, then the rarity of features associated with nozzles is likely just a reflection of nozzle rarity. However, normalization is not possible for permutation analysis of landform nesting. Instead, nesting question 4c from Table 1 was posed to ask specifically what each bankfull landform type was preferentially nested in and what landform type was preferentially nested within it? The top two permutations were tallied out of the five possible in each case.

Results

Bed and width variability and covariance

Analyses in this section characterize the stage-dependent structure of fluvial topographic deviation from central tendency. Overall, the study segment had about a quarter of its stations with extremely high and low Zs values, and this increased slightly with Zd stage (Table 4a). The lowest stage had the most Ws variability and the highest

Table 4. Topographic variability and GCS metrics.

Metric	Zd stage 1	2	4.6	7	9	13	17.6
(A) Topographic variability metrics							
% Abs(Zs)>1	23	26	26	26	26	27	27
% Abs(Ws)>1	30	29	23	20	21	19	16
r*	-0.62	-0.50	-0.16	0.06	0.10	0.13	0.18
(B) Geomorphic covariance metrics**							
Mean Zs·Ws	-0.62	-0.50	-0.16	0.06	0.10	0.13	0.18
% Zs·Ws > 0	30	34	47	52	55	53	55

*Pearson's product-moment correlation (r) values for Ws and Zs. Blue and red shading indicate the highest and lowest values in each column. Grey shading indicates negative r-values that are not the lowest.

**Dark shading indicates values below hypothesized detrended elevation (Zd) threshold.

stage the lowest Ws variability (Figure 6). Ws variability dropped abruptly when Zd stage increased from 2 to 4.6.

The study segment had significant Zs and Ws variability, but the question remained as to whether the sequencing of variability was random. The expectation is that fluvial landforms are identifiable because topography is not randomly ordered, but testing this idea is important. Wald-Wolfowitz runs tests indicated that all segment and reach Zs and Ws longitudinal series were nonrandom above the 99.99% confidence level.

The final test of topographic variability involved ascertaining whether width and bed elevation series are correlated (Table 4). This is the first key test of the study hypothesis. The lowest three stages had negative correlations that were increasingly negative at lower stages. The four highest stages had positive correlations, with correlation strength increasing with stage.

Geomorphic covariance metrics yielded results consistent with those obtained by examining each variable alone. Mean Zs·Ws values were relatively small, but they monotonically increased with stage and switched from negative to positive between Zd stages of 4.6 and 7 m (Table 4). This is also the stage transition at which the proportion of stations with Zs·Ws > 0 exceeded 50%. The segment-scale peak of these two metrics occurred at 17.6 and 9 m, respectively.

Landform abundance

Landform abundance analysis found that topography is simpler and more organized than expected for a confined mountain river (Table 5). For the two lowest Zd stages analyzed, 62 and 65 % of stations were classified as "normal channel" based on their

Table 5. Analysis of landform composition of river as a function of flow. Light grey indicates higher abundance of each type of deep landform. Dark grey indicates higher abundance of each type of shallow landform.

	% of XS locations				
Zd	O	CP	NC	WB	NZ
1	12	1.4	62	3.3	21
2	11	2.5	65	3.8	18
4.6	5.4	8	67	7	13
7	3.7	9.6	71	6.2	10
9	4.6	10	70	7.3	7.5
13	5.4	11	70	7.1	6.0
17.6	5.3	11	71	7.1	5.7

*O=oversized, CP=constricted pool, NC=normal channel, WB=wide bar, NZ=nozzle.

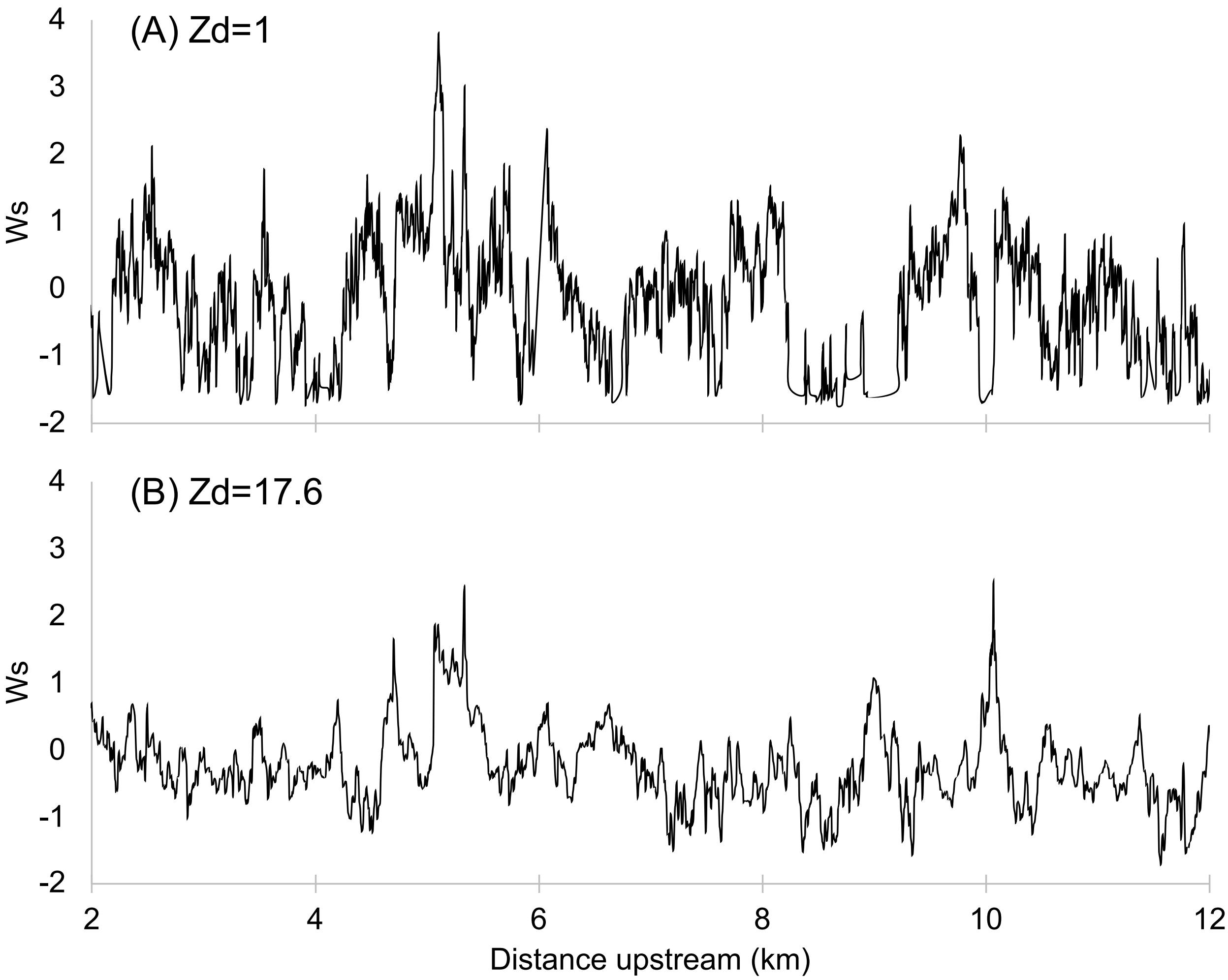
(A) Zd=1
Ws
4
3
2
1
0
-1
-2
(B) Zd=17.6
Ws
4
3
2
1
0
-1
-2
2
4
6
8
10
12
Distance upstream (km)

Figure 6

Zs·Ws occurring within the range of -0.5 to 0.5. The majority of the river's cross-sectional geometry did not deviate strongly from average conditions. As Zd stage increased, the percent normal channel increased and leveled off at 70-71%.

Among landforms representing variable topography, nozzle had the highest abundance at the lowest Zd stage, followed by oversized (Table 5). Their percentages generally declined with increasing Zd stage but not at the same rate. Wide bar and constricted pool had extremely low abundances at low Zd stage, and these values increased with Zd stage, also not at the same rate. Wide bar never exceeded an abundance of 7.3% of the river segment. Constricted pool reached a maximum abundance of just 11%. Overall, these two metrics both showed a threshold change consistent with the study hypothesis (i.e., abundance of CP>O and WB>NZ), but the Zd stage of the thresholds are different from each other and different from that found in the previous three metrics (Table 2).

Landform sequencing

When considering the percent occurrences of transitions > 43% or < 23%, the study found no investigated Zd stage at which the river showed a dominance of specifically nozzle-to-oversized sequencing at low flow and wide bar-to-constricted pool sequencing at high flow (Table 6). Constricted pool was rarely followed by wide bar, though that transition did occur more frequently at higher flows. Instead, constricted pool was predominantly followed by nozzle. In turn, nozzle was most commonly followed by constricted pool, though secondarily it was followed by wide bar. Finally, oversized

Table 6. Longitudinal sequencing of landforms, excluding normal channel units. Shading indicates values > 10% above random expectation.

	% of times unit			
Starting unit	O	CP	WB	NZ
(A) Zd = 1 m				
O		40	30	30
CP	44		6	50
WB	53	13		33
NZ	30	30	40	
(B) Zd = 2 m				
O		39	44	17
CP	33		5	62
WB	62	8		31
NZ	20	65	15	
(C) Zd = 4.6 m				
O		69	31	0
CP	26		19	56
WB	40	33		27
NZ	5	63	32	
(D) Zd = 7 m				
O		56	44	0
CP	16		21	63
WB	33	39		28
NZ	6	41	53	

	% of times unit			
Starting unit	O	CP	WB	NZ
(E) Zd = 9 m				
O		50	50	0
CP	18		29	53
WB	41	35		24
NZ	8	46	46	
(F) Zd = 13 m				
O		29	71	0
CP	15		25	60
WB	57	19		24
NZ	0	71	29	
(G) Zd = 17.6 m				
O		21	79	0
CP	4		23	73
WB	69	27		4
NZ	5	75	20	

preferentially transitioned to constricted pool at low Zd stage and to wide bar at high Zd stage.

To visualize landform sequencing in a simplified schematic for both hypothesis and observed data among all stages, Figure 7 compares them using a box for each landform type and a directed arrow leaving each box that indicates what that landform transitions to downstream. When two landforms alternate sequentially downstream, then the arrow must be bidirectional, as they transition to each other. Thick versus thin arrows in Figure 7b differentiate quantitative results such that transitions with high percent occurrences reveal primary sequencing (thick arrows) and those present but with low percent occurrences reveal secondary sequencing (thin arrows). Figure 7b integrates results across all stages as a first, simplified evaluation. Table 2 calls out a predominance in O-NZ sequencing for low stages and WB-CP sequencing for high stages. That is specifically tested on a stage-basis in subsequent results. Even though O and NZ ought to be rare at high stages (and conversely WB and CP rare at low stages), they should still occur. In such instances, their pairing is assumed as a null hypothesis. Hence, the first test evaluates the status of results across all stages. The schematic clearly and simply differentiates the hypothesis from the observational outcome. In fact, the two pairings were not found to predominate across all stages, necessitating a stage-based inquiry next.

While the simple schematic addresses the test of this study’s scientific hypothesis, other visual representations of landform sequencing help geomorphologists understand how landforms are longitudinally organized as a function of stage. Longitudinal profiles of Zs·Ws colored by landform type show the predominance of nozzle and oversized at

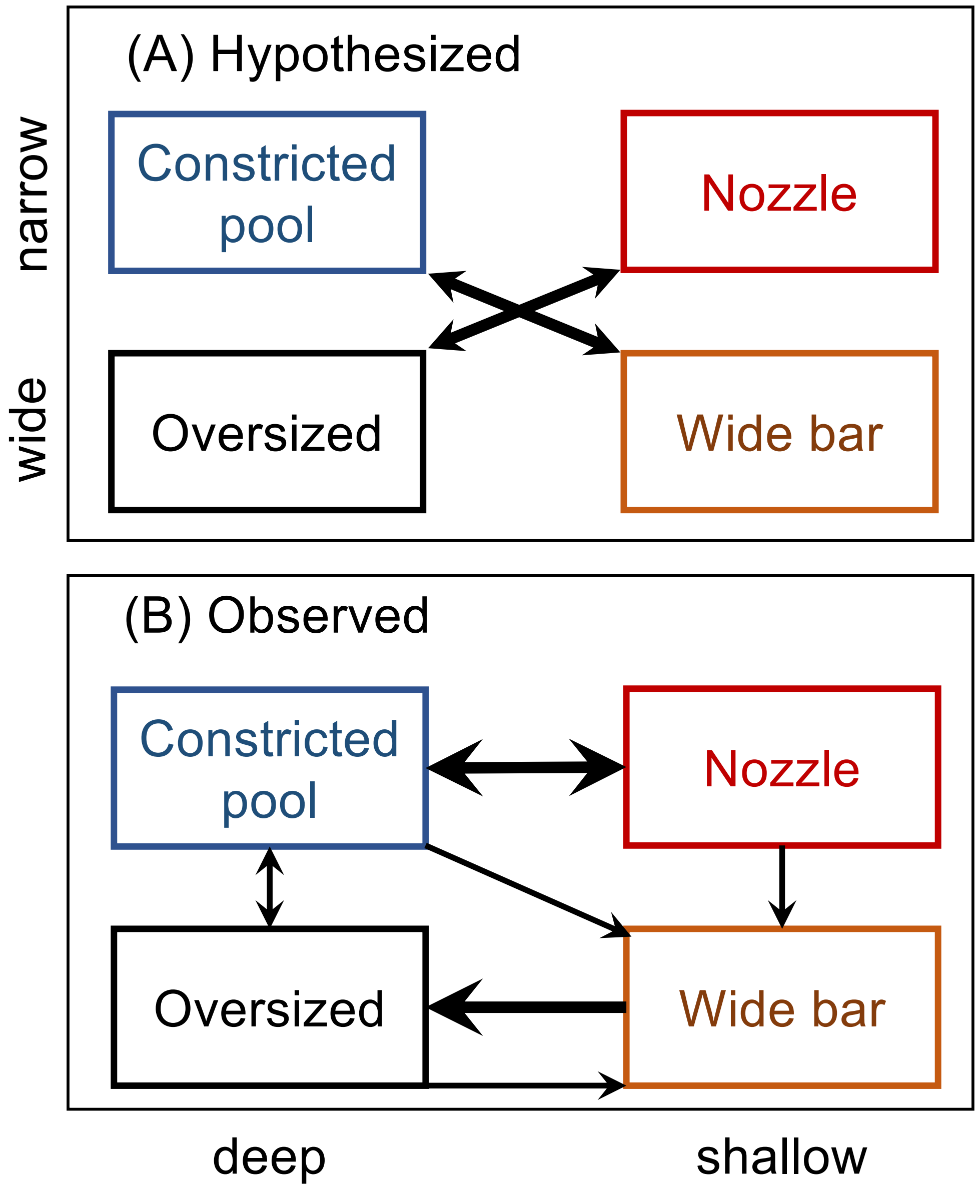
(A) Hypothesized
narrow
wide
Constricted pool
Nozzle
Oversized
Wide bar
(B) Observed
Constricted pool
Nozzle
Oversized
Wide bar
deep
shallow

Figure 7

the two lowest Zd stages (Figure 8) as well as the increased role of wide bar and constricted pool at high Zd stages (Figure 9). Visually, these plots capture many of the hypothesis test metrics and appear to corroborate the study hypothesis as a whole, even though the sequencing test failed to corroborate the hypothesis quantitatively. For example, Figure 8a visually shows a scattering of constricted pool and wide bar units in what is otherwise a river segment dominated by nozzle and oversized units. Perhaps there is just enough of the former units to spoil quantitative transition statistics. However, a visual comparison of all landform profiles (Figures 8-9) going from lowest to highest stage provides a strong impression of the switch from nozzle-oversized dominance to wide bar-constricted pool dominance, which is also indicative of landform nesting, because each stage’s landforms occur within the next higher stage’s landforms.

The third representation of landform sequencing is provided by Sankey diagrams to evaluate differences among base, bankfull, and flood stages (Figure 10). For each landform, on the left, the relative thickness of the connections with the landforms on the right indicates relative abundance of that transition. As stage increases, more constricted pools transition to wide bars (and the same for the converse), matching the hypothesis, but that is not the primary connection. Further, only at base flow do oversized units transition to nozzle. Nozzle transitions to oversized for all three stages, but those transitions are abundant only at base flow. Again, these results match the study hypothesis, but numerically come out secondary to other sequencing.

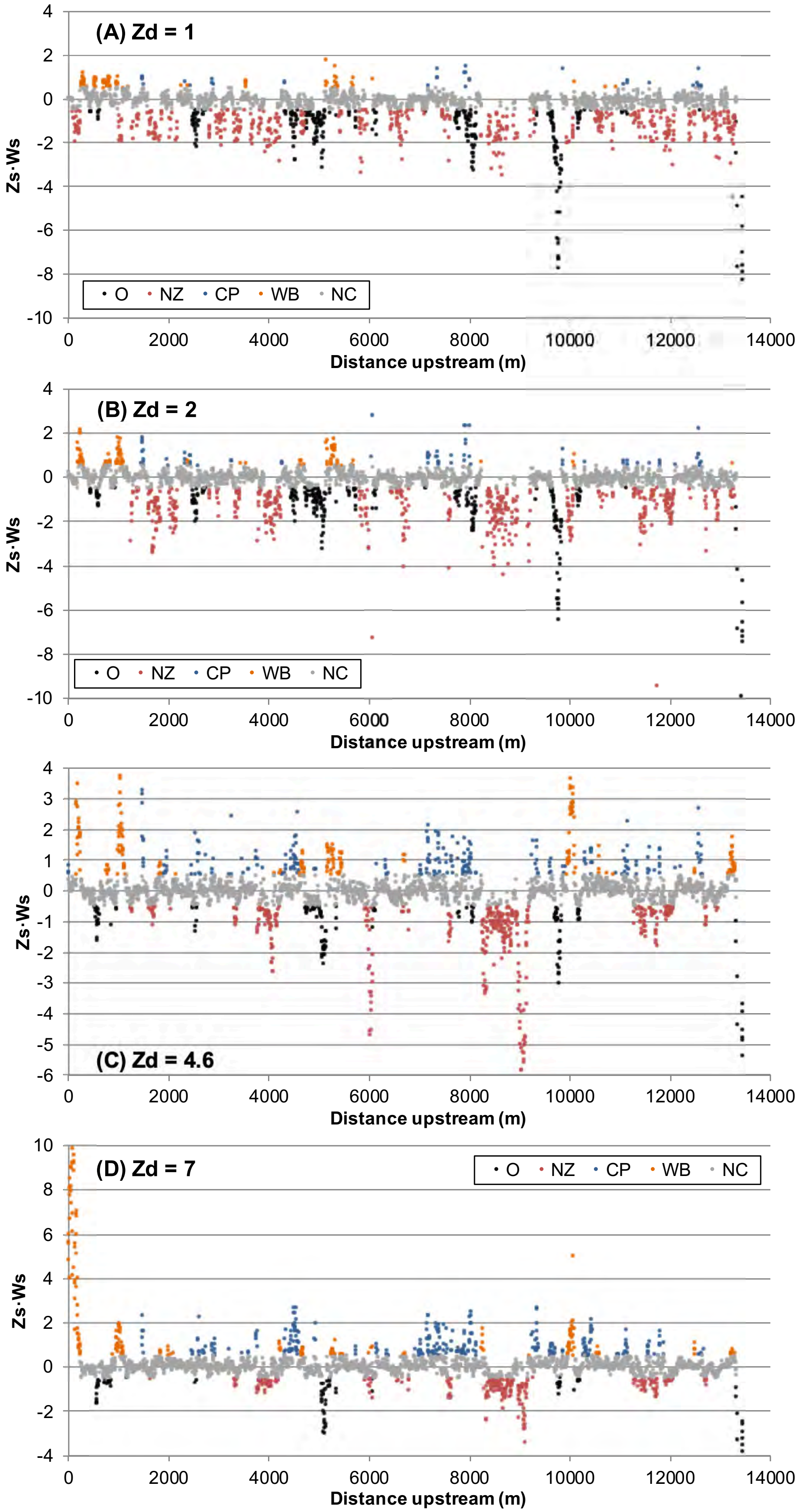

Figure 8

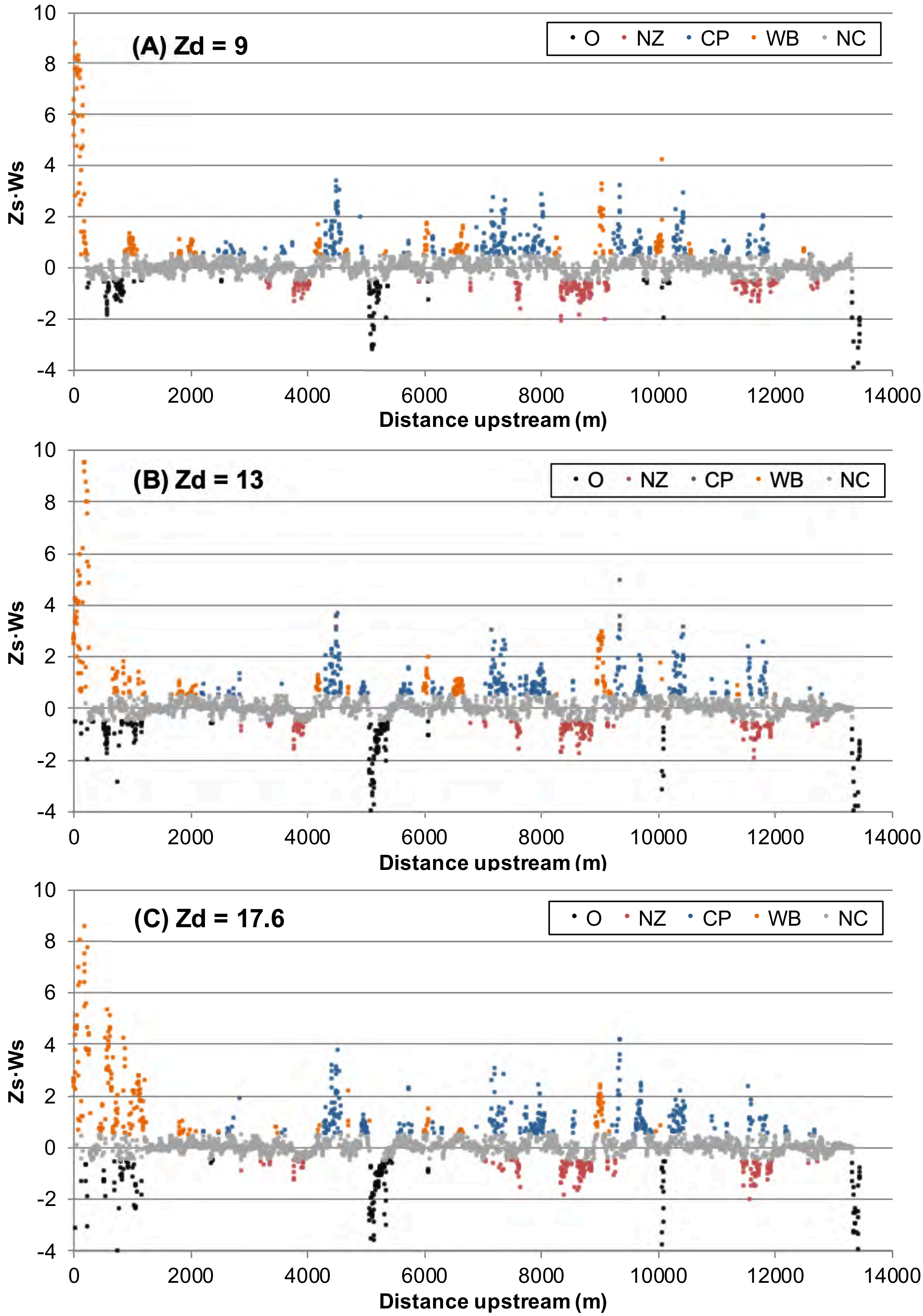
(A) Zd = 9
O
NZ
CP
WB
NC
Zs·Ws
Distance upstream (m)
(B) Zd = 13
O
NZ
CP
WB
NC
Zs·Ws
Distance upstream (m)
(C) Zd = 17.6
O
NZ
CP
WB
NC
Zs·Ws
Distance upstream (m)

Figure 9

Landform nesting

Of 125 possible permutations of landform nesting, 51 permutations had at least 1 occurrence, while 74 did not occur. Four examples are illustrated in Figure 11. The most common permutation by far was the strictly defined normal channel across all flows, which occurred for 39% of stations. The second most common occurrence (11%) was a baseflow nozzle nested in normal bankfull and floodprone channels. The third most common (5.4%) was nozzle at all flows (Figure 10a). Nozzle-nozzle-nozzle nesting was the top permutation with topographic nonuniformity across all flows. Two nesting patterns are tied in fourth place (4.0%); they are nozzle at baseflow and bankfull flow nested in normal channel at floodprone flow and normal channel at baseflow and bankfull flow nested within constricted pool at floodprone flow.

The next step of the landform nesting analysis evaluated the top three permutations of bankfull and baseflow landforms nested in each of the floodprone landform types (Table 7). Nozzle, normal channel, and oversized had the nesting of persistently identical landform types (e.g., nozzle within nozzle within nozzle) as the top nesting permutation at the floodprone scale. The second most abundant permutation for nozzle and normal channel again had the same type at the bankfull stage as at the floodprone stage, indicative of their persistence with stage in many locations. For its top permutation, floodprone wide bar had bankfull wide bar nested within it, and interestingly baseflow nozzle was nested within that. Figure 11c shows a similar case with nozzle in nozzle in wide bar, driven by large boulders dividing flow into separate chutes and limiting bankfull width.

Table 7. Top three permutations of hierarchical nesting of flow convergence routing landforms within the five floodprone landform types.

Zd = 9	Zd= 4.6	Zd = 1	Count	% of river
(A) Nested within floodprone nozzle				
NZ	NZ	NZ	160	5.4
NZ	NZ	NC	33	1.1
NZ	NC	NC	18	0.6
(B) Nested within floodprone wide bar				
WB	WB	NZ	52	1.8
WB	NC	NC	48	1.6
WB	NC	NZ	44	1.5
(C) Nested within floodprone normal channel				
NC	NC	NC	1161	39
NC	NC	NZ	338	11
NC	NZ	NZ	119	4.0
(D) Nested within floodprone constricted pool				
CP	NC	NC	118	4.0
CP	CP	NC	80	2.7
CP	NC	O	56	1.9
(E) Nested within floodprone oversized				
O	O	O	59	2.0
O	NC	WB	21	0.7
O	NC	NC	20	0.7

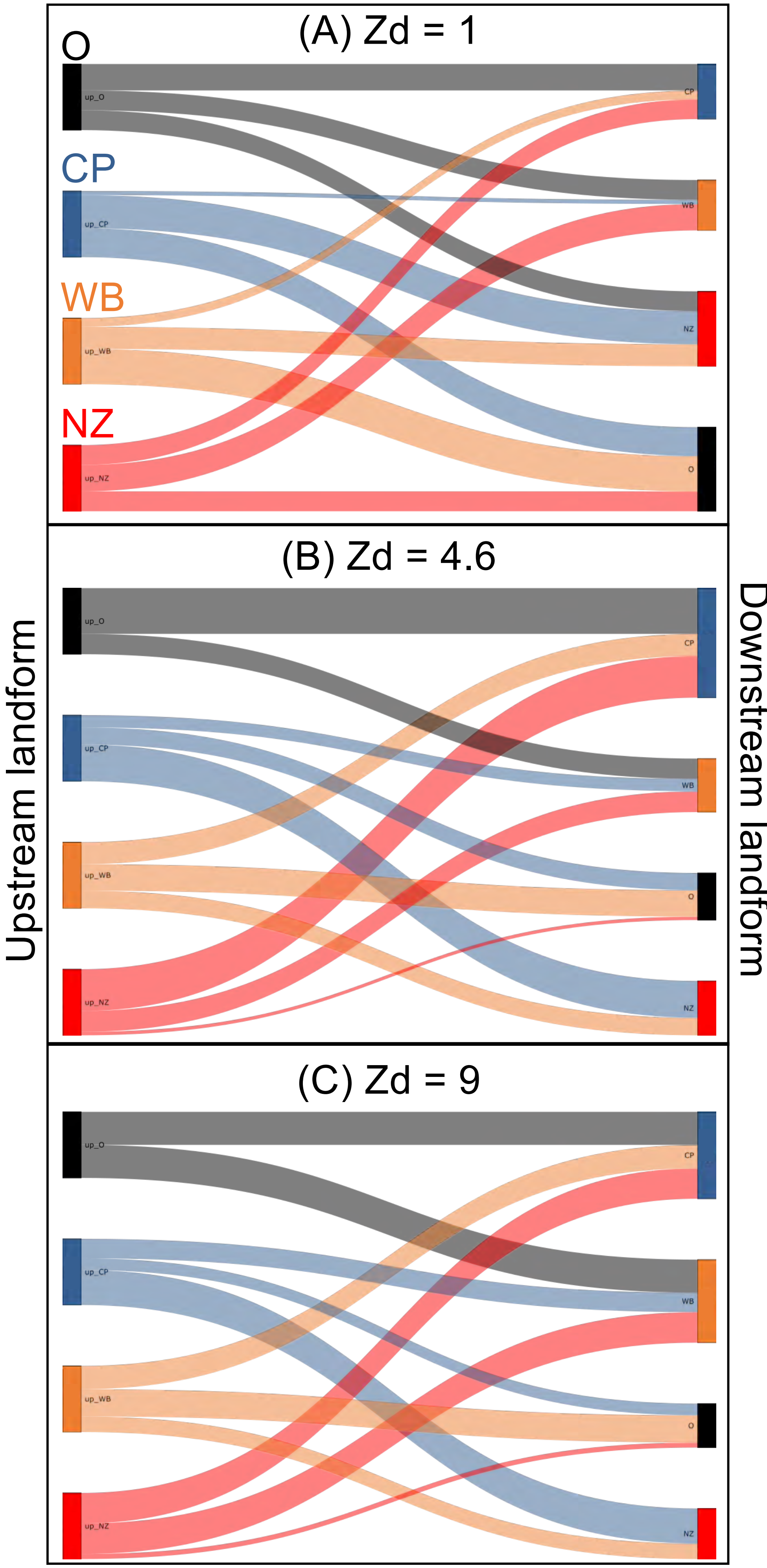
(A) Zd = 1
(B) Zd = 4.6
(C) Zd = 9
O
CP
WB
NZ
up_O
up_CP
up_WB
up_NZ
Upstream landform
Downstream landform

Figure 10

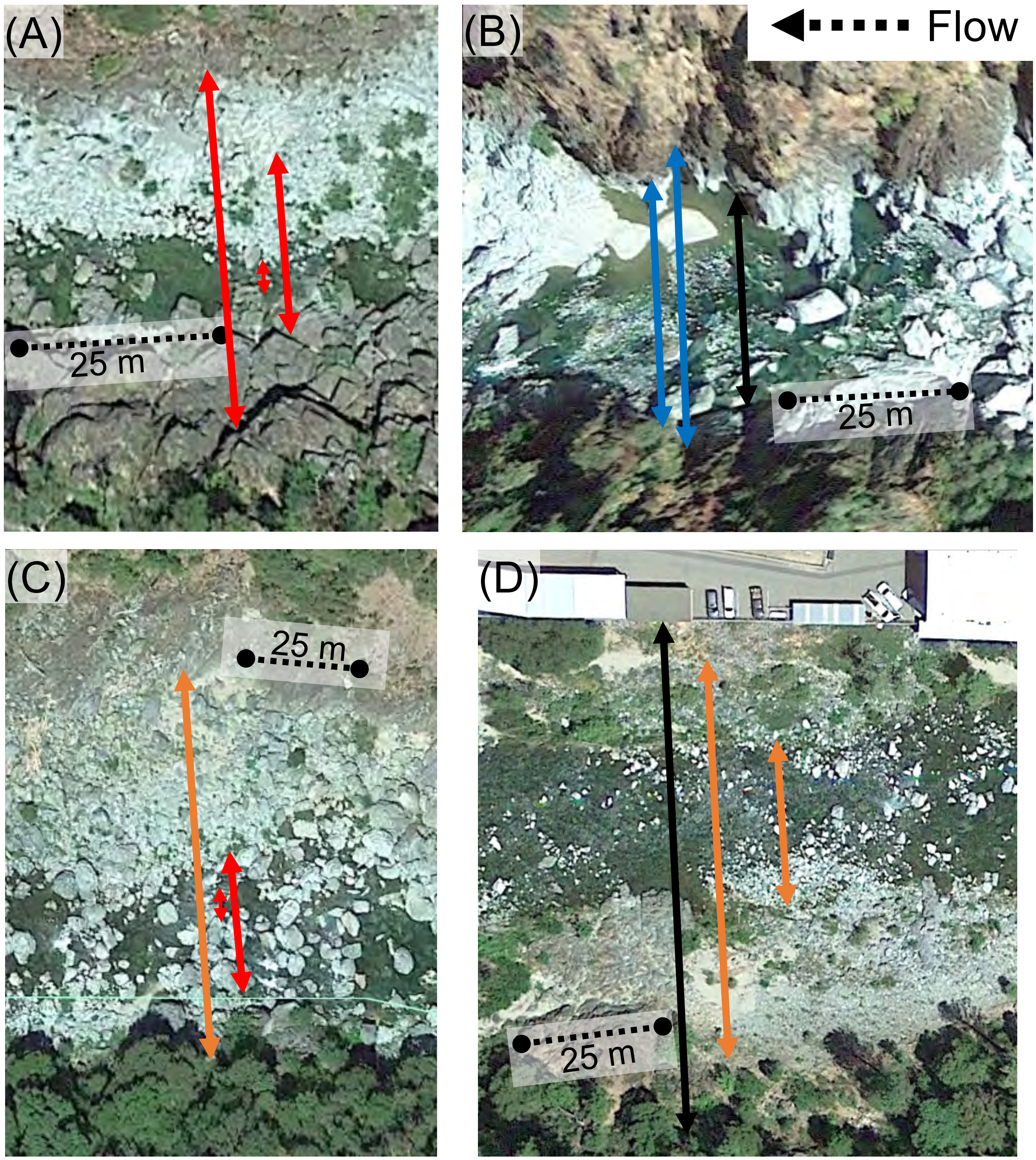

Figure 11

Because classic cross-sectional area and velocity reversal theory anticipates a two-stage FCR mechanism, the expectation follows that wide bar and nozzle landforms acting as riffles at base flow should be nested within wide bar bankfull landforms (e.g. Figure 11d). In fact, nozzle nested within wide bar was the top permutation but wide bar nested within wide bar was only ranked third after normal channel within wide bar. Further, oversized and constricted pool baseflow landforms should be nested within constricted pool bankfull landforms (e.g., Figure 11b). This time, normal channel nested within constricted pool was the top permutation and oversized in constricted pool ranked second. Thus, hypothesis expectations were mostly met but it is difficult to interpret the higher presence of normal channel than expected. Meanwhile bankfull nozzle and oversized tended to have their own type nested within them preferentially, followed by having normal channel nested within them (Table 8).

The final hierarchical nesting analysis assessed what floodprone landform type each bankfull landform type was nested within. The study hypothesis has no specific expectation for this analysis. Again, the top two permutations were tallied (Table 8). Nozzle, normal channel, and constricted pool bankfull landforms were preferentially nested within themselves at the floodprone scale. The rest were nested within normal channel.

Table 8. Top two permutations of hierarchical nesting of bankfull landforms, either within (A-E) or beyond (F-J) them.

Test 1: within bankfull landform

Zd = 4.6	Zd= 1	Count	% of river
(A) within bankfull nozzle			
NZ	NZ	293	10
NZ	NC	81	2.8
(B) within bankfull wide bar			
WB	NZ	109	3.7
WB	NC	78	2.7
(C) within bankfull normal channel			
NC	NC	1365	46
NC	NZ	392	13
(D) within bankfull constricted pool			
CP	NC	163	5.5
CP	O	47	1.6
(E) within bankfull oversized			
O	O	132	4.5
O	NC	19	0.6

Test 2: what each bankfull landform is nested within

Zd = 9	Zd = 4.6	Count	% of river
(F) hosting bankfull nozzle			
NZ	NZ	193	6.6
NC	NZ	152	5.2
(G) hosting bankfull wide bar			
NC	WB	111	3.8
WB	WB	69	2.3
(H) hosting bankfull normal channel			
NC	NC	1623	55.1
CP	NC	182	6.2
(I) hosting bankfull constricted pool			
CP	CP	117	4.0
NC	CP	108	3.7
(J) hosting bankfull oversized			
NC	O	80	2.7
O	O	76	2.6

Discussion

Threshold stage found?

Mountain rivers require significantly higher discharges at longer recurrence intervals than lowland rivers for maintenance of landform sequences (Grant et al., 1990). This observation is ascribed to the presence of macro-roughness features, such as coarse sediment and large woody materials that extract energy from the flow and are only mobilized or destabilized at these high discharges, as well as exposed bedrock surfaces that are resistant to erosion (Bathurst, 1978). This study presents a different way of thinking about and querying the controls on stage-dependent morphodynamics, bringing the topographic regime into the foreground.

Whether or not a river has a bankfull discharge and whether such a flow controls anything are not the relevant questions within the GCS framework. Nor is it relevant to understanding landform structure to ask what discharge is associated with incipient entrainment of bed sediment. Instead, the approach begins with a single morphodynamic mechanism and tests whether or not the observed spatial pattern of landforms is consistent with a dominant role of that mechanism.

This study posed a specific question about the range of discharges for which a mountain river’s landform assemblage is freely self-maintaining. It stated a specific hypothesis as to how the question would be answered, given a specific morphodynamic mechanism. Eight specific metrics from GCS analysis were used to test aspects of the hypothesis (Table 2). Five of the six metrics specifically designed to test for the presence of a threshold change in mountain river topography as a function of spatial scale did find a threshold and the directionality of change was as expected. The three broadest metrics indicated the threshold occurs between a Zd stage of 4.6 and 7 m. Of these, the two Ws·Zs metrics further indicate that landform organization continues to re-organize toward a more freely self-maintaining structure up to a Zd stage of 9. Above that stage results remain stable. The landform abundance metric focusing on topographic troughs found the threshold change from wide (O) to narrow (CP) landforms to occur at a lower Zd stage between 2 and 4.6 m. The metric focusing on topographic ridges found the threshold change from narrow (NZ) to wide (WB) landforms at a much higher Zd stage between 9 and 13 m. Inevitably there are nuances between metrics given that rivers typically experience multiple processes concurrently and the topographic regime varies by reach.

To a large degree (but not entirely), study results corroborate the hypothesis that there exists a threshold stage in topographic structure consistent with FCR morphodynamics, thereby affirmatively answering the study question. Flow convergence routing seems to not act alone in the confined Yuba River, but this mechanism has definitely left its signature. More studies are needed across diverse confined mountain rivers to ascertain how broadly study conclusions apply and to better understand landform sequencing and nesting.

Nevertheless, GCS analysis can be used to detect a threshold change in wholesale landform organization in a mountain river in relation to an important morphodynamic mechanism playing a role in shaping that organization. Further, GCS analysis shows that as a valley fills with water, the topographic regime (and its control on hydro-morphodynamics) is not static but dynamic due to the multiple scales of topographic variability present. Only at discharges above the diagnostic threshold is the landscape structured in a way where depth and width undulations are in sync. The magnitude of this threshold is expected to vary with channel type.

Ultimately, the main point is that a person looking at a confined mountain river may be drawn to charismatic large bed elements in the baseflow domain and wonder about their importance. Instead, this study suggests that what is remarkable about mountain rivers is that above a threshold stage a whole new terrain comes into focus, and with it a completely different set of associated fluvial dynamics. This is nested on top of the baseflow structure. Understanding the threshold and nesting between these regimes should be an important goal of fluvial geomorphology in the 21st century.

Reduced role of bankfull discharge

Study results have implications for the concept of bankfull discharge applied to mountain rivers, because the transition to freely self-maintaining landform organization is never as low as the Zd stage of 2 m estimated as bankfull stage by YCWA (2013). It may be that a bankfull channel dimension exists, either identified by the statistical definition of bankfull flow or geometric indicators of flow just filling a U-shaped channel up to a lateral slope break. It is commonly recommended that bankfull discharge in mountain rivers be estimated using a range of recurring discharges based on several field indicators (Radecki-Pawlik 2002). However, whether such stages have anything to do with a single, special “channel-forming” flow that controls the topographic structure of the river is highly suspect.

Similar to the findings of this study, the GCS analysis of the partially confined, gravel-cobble lower Yuba River by Pasternack et al. (2018b) concluded that topographic structure had to be controlled by a discharge significantly higher than bankfull flow. Those results were backed up by 2D bed shear stress predictions for a wide range of discharges, showing that wholesale organization of riffles and pools could not be achieved by flows of 1-2 times bankfull discharge. Similarly, Sawyer et al. (2010) showed that it took a discharge of ~ 7.6 times bankfull to scour pools and deposit sediment on riffles in one reach of the lower Yuba River. Thus, even though a threshold change in river topography as a function of spatial scale may occur at or close to bankfull discharge, the channel-forming flow causing that change appears to be significantly higher. This requires more process-based research using numerical modeling and physical experiments.

Mountain river “complexity”

Mountain rivers are often thought of as "highly complex", but that impression comes from the visual charisma of large bed elements, tumbling and turbulent flows, and multi-threaded flow paths; whether the underlying landform structure is complex or not has not been well studied. This study illustrates that it is possible to turn the poorly conceptualized idea of “complexity” into specific, quantifiable metrics. For example, complexity can be quantified in terms of the number of standard deviations away from average values variables are at points along spatial series. It can also be quantified in terms of the abundance, sequencing, and nesting of scale-independent landform types. In this study, the mountain river was found to have the normal channel landform type at

62-71% of 2944 cross-sections across base flow to a flood with a 36-year recurrence interval. By comparison, the abundance of normal channel for the lower Yuba River segment in 2008 was 36-62% considering similar baseflow to moderate flood stages (Pasternack et al., 2018b). Constricted pool abundance was quite low compared to the partially confined gravel-cobble lower Yuba River and literature addressing the importance of pool constrictions in mountain rivers (Thompson et al., 1999). These landform abundance values suggest that many of the positive values of Zs·Ws that occur are < 0.5, and therefore classified as normal channel. By comparison, the abundances of wide bar and constricted pool for the 2008 lower Yuba River are ~ 16-20% and ~ 16-25%, respectively. As a whole, the mountain river was relatively uniform in terms of its underlying landforms, and where it was not uniform it had an abundance of nozzle and oversized units. The primary explanation for the overall lack of complexity is that mountain rivers are confined by canyon walls and therefore lack the width variability necessary to exhibit high complexity relative to partially confined rivers that can have landform types spanning unconfined to confined corridor settings.

Challenges posed by sequence and nesting analyses

While landform sequencing studies have been done (e.g., Grant et al., 1990; Wyrick and Pasternack, 2014), the approach is underutilized and therefore can prove difficult to conceptualize. In this study, the hypothesis offered a relatively simple alternation between two landforms types at low stage (NZ-O) and two at high stage (WB-CP). Visually, a simple alternation seems present in Figures 8 and 9. However, landform sequencing in the Yuba River was often dictated by canyon confinement. Narrow canyon sections had alternating sequences of constricted pool and nozzle. In that setting, sediment scoured out of a constricted pool likely would not be routed to and deposited on the next downstream unit, but instead would move quite a way downstream before the canyon finally widens enough to allow deposition. The fact that nozzle was followed by wide bar preferentially at 2 stages suggests that in those cases that nozzle-to-wide-bar marks the transition from a narrow to wide canyon or a tributary junction. This sequencing is unexpected, because width transitions often have hydraulic jets that cause deep scour, and that ought to yield a constricted pool or oversized unit. Perhaps the jet can be short and localized enough at the entrance of an expansion to not affect the entire cross-section. The implication is that sediment moving down the river is accumulating farther downstream and when the valley does eventually widen this materials is deposited suddenly, regardless of any jet, to form wide bar units with almost no channel-wide scour hole.

A unique and important feature of GCS analysis is that it enables evaluation of the spatial nesting of the same set of landform types within themselves. Classically, one would never say that a riffle was nested in a pool or even nested within a riffle. The classic terms of riffle, pool, run, and glide are inherently scale dependent (Frissell et al., 1986), are descriptive based on local conditions, and therefore are not definitive of a hydraulic or geomorphic process. Geomorphic understanding of these terms primarily arises through statistical correlations between expert-identified units and whatever other ecologic, hydraulic, or geoscientific attribute is of interest. As a result, the ability to evaluate how process-relevant landforms nest within themselves contributes to understanding spatial scaling in fluvial geomorphology.

The results of three-stage nesting analysis using all five landforms in the mountainous Yuba River found that nesting permutation frequencies mimic landform abundance. Because normal channel is the most abundant landform at all stages and nozzle is the second most abundant landform at four stages (Figures 8-9), a higher probability exists that normal channel and nozzle nesting permutations are most abundant. That means that it is plausible that stochasticity governs three-stage nesting when normal channel landforms are included in consideration. In other words, the sheer abundance of normal channel units in the confined canyon river segment is overwhelming local FCR signals when related to the other landforms, when all data from a long segment is analyzed together. In the absence of the same kind of large width undulations as present further down a mountain where canyons give way to partially confined valleys (Pasternack et al., 2018b), the river corridor has many sub-reach scale intervals that are relatively monotonous normal channel, and these will not experience FCR morphodynamics. As stated throughout this article, FCR is one of many processes in a river. Even at the discharges where FCR drives freely self-maintaining landform organization of wide bar and constricted pool units, there are still long intervals of normal channel where FCR is not active. This study now quantifies and clarifies the limited extent of FCR for a confined mountain river.

The results of two-stage nesting analysis of bankfull and baseflow landforms nested in each of the floodprone landform types found that at base flow the wide bar floodprone landform is dissected with narrow, shallow chutes making a bar-chute complex. This complex structure can drive stage-dependent convergence and divergence of flow consistent with the study hypothesis. Meanwhile, the floodprone constricted pool landform tended to have a lot of normal channel nested within it, which is sensible because the canyon is too narrow to support nesting of oversized and wide bar base flow units.

In partially confined and unconfined reaches of the lower Yuba River, Pasternack et al. (2018b) found a diversity of landform nesting, but especially that baseflow and bankfull landforms appear controlled by what landform they are nested in at the floodprone area spatial scale. That is not the case in the mountains. Instead, the dominant nesting structures involved the same unit type occurring at all three spatial scales due to canyon confinement (e.g., nozzles within nozzles within nozzles). Where floodprone wide bar units existed, they tended to have normal channel and nozzle units within them, often involving a bar-chute structure. This is not especially profound, but it does define the fundamental hierarchical nesting signature of a canyon-confined mountain river. The finding that the same landform type tended to nest within itself down the three scales indicates that at the high stages no new forms of topographic variability are being encountered up the canyon walls; the canyon setting of wall undulations or lack thereof is essentially set.

Other processes are important

It is important to take note that even though FCR enables freely self-maintaining landform organization for stages > 4.6 m in this river, other important processes likely play a secondary role. For example, the stage-independent presence of oversized landforms at a few locations is likely diagnostic of a positive-feedback morphodynamic mechanism in which sediment “tools” and plunging flows carve deeper and deeper over time, with no resetting mechanism (Sklar and Dietrich, 2006). Tributary junctions and hillside-channel connectivity also exert significant controls on river corridor geomorphology (Benda et al., 2004; Korup and Schlunegger, 2007). In this way, GCS analysis can be meaningful not only for affirming the presence of a process, but for identifying key locations where that process is not relevant and directing alternative analysis to focus there. It can also spur conceptualization of new processes that reflect or can mechanistically explain the observed landform patterns.

Broader significance

Fluvial geomorphology in the 20th century focused on ascertaining the central tendency of morphological attributes and empirically linking mean values to hydrologic, hydraulic, and sediment transport variables. Empirical river morphology data is fraught with large variability (Knighton, 1998) – sometimes orders of magnitude – yet it is often ignored, even though two or more patterns of variability can work in concert to produce important morphodynamics and ecohydraulics. At best, spatial variability has been described in geological and landscape contexts (e.g., Keiffer, 1989; Grant et al., 1990). Secondarily, extensive quantitative analysis has focused on descriptive characterization of bed undulation to form riffle-pool or step-pool sequences (e.g., Chin, 1999; Parker and Izumi, 2000; Thompson, 2001).

Today, fluvial geomorphology is rapidly outgrowing the paradigm of statistical sampling with cross-sections in favor of comprehensive mapping and analysis of three-dimensional 'riverscapes' using near-census, meter-resolution remote sensing data (Fausch et al., 2002; Carbonneau et al., 2012; Gonzalez and Pasternack, 2015). This transformation brings the characterization of variability and mechanistic understanding of its role in fluvial processes to the forefront of scientific research. Whether variability in multiple metrics might be coherently structured and how that would influence river classifications could not be assessed with traditional cross-sectional sampling data, because such data are too sparse (Gonzalez and Pasternack, 2015). With modern digital terrain models, the time has arrived to thoroughly assess nested scales of patterns in variability for real river datasets.

As always, artificial rivers constructed in physical experiments play a critical role in understanding morphodynamics and addressing process-form linkages. They offer the best opportunity to directly observe change and infer processes under known conditions (Kleinhans, 2010; Chartrand et al., 2018). However, due to scaling constraints and design limitations their results can be difficult to translate to the environments they mimic. Studies of the complexity of real rivers must go hand-in-hand with those of simplified flume channels. At the very least, GCS analysis of real rivers can help check and elucidate findings from flume studies by providing a well-defined framework for examining organized variability in natural rivers.

One path forward may be to build upon classic statistics by advancing new descriptive metrics using geostatistics and artificial intelligence (e.g., Beechie and Imaki, 2014; Bugnicourt et al., 2018; Clubb et al., 2019). These metrics have mathematical meaning, but often they have no immediate geomorphic meaning, eventually necessitating more statistics to correlate new statistical metrics to geomorphic metrics. The risk is that through overfitting using massive datasets, seemingly predictive models will arise and be published in multitude as a new variation on the p-hacking controversy

(Head et al., 2015), such as when a few positive results are cherry picked out of many negative ones or when very low explanatory power is present as a statistical fluke but results are published for technically reaching 95% statistical confidence. Yet all these statistics upon statistics will not yield a mechanistic understanding of how landforms respond to and control fluvial morphodynamics and other essential environmental dynamics. Statistics work best when they used to test specific links in a mechanistic chain one at a time, such as in each small test in Table 1.

The concept of a geomorphic covariance structure offers just such a compromise between staying true to mechanistic science while still receiving the benefits of statistical methods. Variations found in nature are often not stochastic but include strong deterministic patterning. The GCS framework offers a way to capture patterning down a river, relying solely on statistics for the purposes of determining presence/absence and describing the degree of explanatory power explained via straightforward physical understanding of morphodynamics.

The way the GCS framework achieves a mechanistic focus is by casting the results in terms of a set of five scale-independent, nestable landforms associated with a specific mechanism. In the case of this study, the GCS involves spatial series relevant to FCR morphodynamics. This is not the only process that can be assessed with the GCS framework, but it is the one selected for study in the mountainous Yuba River.

River restoration based on classic empirical geomorphology emphasizing reach-average central tendencies (e.g., Rosgen, 2006) is widely regarded as a failure by academics who have thoroughly investigated restoration outcomes (Palmer et al., 2005, 2010; Roni et al., 2008; Simon et al., 2008). Academic geomorphologists have reached a consensus that restoration should be focused on re-initiating natural processes (Beechie et al., 2010; Wohl et al., 2015). How can restoration practitioners literally design a process? The key is recognizing that the mechanistic chain of events we term a “process” (Wheaton et al., 2004; Pasternack, 2020a) is fundamentally controlled by synergistic hydrologic, topographic, and sedimentary variability. For example, imagine a channel designed exactly to empirical specification using reach-average metrics with no bed, width, or centerline curvature undulations. Often the intention is to have no change at all such that the channel exactly passes the sediment it receives. However, when the flow rises in that channel, the only processes that can occur given a sediment imbalance are bed incision and bank collapse; hardly the scope of what is needed for a natural channel. Over time, enough bed and bank failure may transform the channel to have GCSs that can then begin to instate meaningful morphodynamics, but this is environmental stewardship by blindfolded ignorance and prayerful hope (Pasternack, 2020a).

In contrast, when a channel is designed with a suite of GCSs, one can mindfully institute a wide range of potential morphodynamic mechanisms and have confidence they will be self-maintaining. To help practitioners use GCSs in river design, Pasternack and Zhang (2020) presented the free, open-source Python3 software called River Builder, available at GitHub. The latest version has a multitude of types of variability functions that can be applied in as detailed of a nested spatial hierarchy from shallowest inner channel to edge of the valley as one wants. Consequently, GCS theory stands apart from classic statistical geomorphic analysis in that it not only helps comprehend how rivers are structured in response to morphodynamic processes, but it is immediately useful as a practical aid in river stewardship. The key next step is to undertake GCS investigations of a wide range of river types.

Conclusions

At the highest level this study used the GCS analyses from Table 1 to test a specific scientific hypothesis using transparent performance indicators identified in Table 2. This experimental design was used to identify a stage threshold in morphodynamic control over fluvial landform structure in a canyon-confined mountain river. It also revealed the self-affine hierarchical nesting structure of canyon-confined fluvial landforms in contrast with previous non-affine nesting in partially confined and unconfined lowland reaches. Geomorphic covariance structure theory and methods have important implications for professional practices in river management and engineering. Practitioners can now mindfully design requisite, linked patterns in depth and width variability across spatial scales to instill morphodynamic processes that are self-maintaining over a wide range of flows.

Acknowledgements

This work was funded by the Yuba Water Agency (Marysville, California, USA; (Award #201503808) and the USDA National Institute of Food and Agriculture, Hatch project number #CA-D-LAW-7034-H. We thank Xavier Nogueira in our lab group for contributing data for us to produce Figure 1. We thank anonymous reviewers for detailed constructive criticism that helped improve the original manuscript.

Data Availability Statement

The data presented in tables and figures that support the findings of this study are available from the first author (http://pasternack.ucdavis.edu) upon request with no restrictions. Restrictions apply to the availability of the underlying digital elevation model, which was used under contractual agreement from the project sponsor for this study. The digital elevation model is available from the first author with the permission of Yuba Water Agency.

Conflicts of Interest

None.

References

De Almeida GAM, Rodríguez JF. 2011. Understanding pool-riffle dynamics through continuous morphological simulations. Water Resources Research, 47(1). DOI: 10.1029/2010WR009170.

Baker VR, Ritter DF. 1975. Competence of rivers to transport coarse bedload material. *Geological Society of America Bulletin* **86** (7): 975-978.

Baker VR, Pickup G. 1987. Flood geomorphology of the Katherine Gorge, Northern Territory, Australia. *Geological Society of America Bulletin* **98**: 635-646.

Bathurst JC. 1978. Flow resistance of large-scale roughness. *Journal of the Hydraulics Division* **104** (12): 1587-1603.

Beechie T, Imaki H. 2014. Predicting natural channel patterns based on landscape and geomorphic controls in the Columbia River basin, USA. *Water Resources Research* **50** (1): 39–57.

Beechie TJ, Sear DA, Olden JD, Pess GR, Buffington JM, Moir H, Roni P, Pollock MM. 2010. Process-based Principles for Restoring River Ecosystems. *Bioscience* **60**: 209-222. DOI: 10.1525/bio.2010.60.3.7

Benda L, Poff NL, Miller D, Dunne T, Reeves G, Pess G, Pollock M. 2004. The network dynamics hypothesis: How channel networks structure riverine habitats. *BioScience* **54**: 413-427.

Bishop, MP, James LA, Shroder Jr JF, Walsh SJ. 2012. Geospatial technologies and digital geomorphological mapping: concepts, issues and research. *Geomorphology* **137**: 5-26.

Brierley GJ, Fryirs KA. 2005. Geomorphology and River Management: Applications of the River Styles Framework. Oxford, UK: Blackwell Publishing.

Brown RA, Pasternack GB. 2014. Hydrologic and topographic variability modulate channel change in mountain rivers. *Journal of Hydrology* **510**: 551-564. DOI: 10.1016/j.jhydrol.2013.12.048.

Brown RA, Pasternack GB. 2017. Bed and width oscillations form coherent patterns in a partially confined, regulated gravel–cobble-bedded river adjusting to anthropogenic disturbances. *Earth Surface Dynamics* **5**: 1-20. DOI: 10.5194/esurf-5-1-2017.

Brown RA, Pasternack GB. 2019. How to build a digital river. *Earth-Science Reviews* **194**: 283-305.

Brown RA, Pasternack GB, Wallender WW. 2014. Synthetic river valleys: Creating prescribed topography for form–process inquiry and river rehabilitation design. *Geomorphology* **214**: 40-55. DOI: 10.1016/j.geomorph.2014.02.025.

Brown RA, Pasternack GB, Lin T. 2015. The topographic design of river channels for form-process linkages for river restoration. *Environmental Management* **57** (4): 929-942. DOI: 10.1007/s00267-015-0648-0.

Bugnicourt P, Guitet S, Santos VF, Blanc L, Sotta ED, Barbier N, Couteron P. 2018. Using textural analysis for regional landform and landscape mapping, eastern Guiana shield. *Geomorphology* **317**, 23–44. DOI: 10.1016/j.geomorph.2018.03.017.

Carbonneau P, Fonstad MA, Marcus WA, Dugdale SJ. 2012. Making riverscapes real. *Geomorphology* **137** (1): 74-86. DOI: 10.1016/j.geomorph.2010.09.030.

Chartrand SM, Jellinek AM, Hassan MA, Ferrer-Boix C. 2018. Morphodynamics of a width-variable gravel bed stream: New insights on pool-riffle formation from physical experiments. *Journal of Geophysical Research: Earth Surface* **123** (11): 2735-2766.

Chin A. 1999. The morphologic structure of step–pools in mountain streams. *Geomorphology* **27** (3-4), 191-204.

Clifford NJ. 1993. Formation of riffle-pool sequences: Field evidence for an autogenetic process. *Sedimentary Geology* **85**: 39-51.

Clubb FJ, Bookhagen B, Rheinwalt A. 2019. Clustering river profiles to classify geomorphic domains. *Journal of Geophysical Research: Earth Surface* 124 (6): 1417-143. DOI: 10.1029/2019jf005025.

Curran JC. 2007. Step–pool formation models and associated step spacing. *Earth Surface Processes and* Landforms **32**: 1611–1627.

Curtis JA, Flint LE, Alpers CN, Yarnell SM. 2005. Conceptual model of sediment processes in the upper Yuba River watershed, Sierra Nevada, CA. *Geomorphology* **68** (3-4): 149-166. DOI: 10.1016/j.geomorph.2004.11.019.

De Almeida, G.A.M. & Rodríguez, J.F. (2011) Understanding pool-riffle dynamics through continuous morphological simulations. Water Resources Research, 47(1), W01502. https://doi.org/10.1029/2010WR009170.

Fausch KD, Torgersen CE, Baxter CV, Li HW. 2002. Landscapes to riverscapes: bridging the gap between research and conservation of stream fishes: a continuous view of the river is needed to understand how processes interacting among scales set the context for stream fishes and their habitat. *Bioscience* **52** (6): 483-498. DOI: 10.1641/0006-3568(2002)052[0483:LTRBTG]2.0.CO;2.

Furbish DJ. 1998. Irregular bedforms in steep, rough channels 1. Stability analysis. *Water Resources Research* **34**: 3635–3648. DOI:10.1029/98WR02339.

Frissell CA, Liss WJ, Warren CE, Hurley MD. 1986. A hierarchical framework for stream habitat classification: viewing streams in a watershed context. *Environmental Management* **10**: 199–214. https://doi.org/10.1007/bf01867358.

Fryirs KA., Wheaton JM, Brierley GJ. 2016. An approach for measuring confinement and assessing the influence of valley setting on river forms and processes. *Earth Surface Processes and Landform*s **41** (5): 701-710. doi:10.1002/esp.3893.

Gilbert GK. 1917. Hydraulic-mining Debris in the Sierra Nevada. US Geological Survey Professional Paper 105, US Geological Survey, Washington, DC.

Grant GE, Swanson FJ, Wolman MG. 1990. Pattern and origin of stepped-bed morphology in high-gradient streams, Western Cascades, Oregon. *Geological Society of America Bulletin* **102**: 340–352.

Gonzalez RL, Pasternack GB. 2015. Reenvisioning cross-sectional at-a-station hydraulic geometry as spatially explicit hydraulic topography. *Geomorphology* **246**: 394-406. DOI: 10.1016/j.geomorph.2015.06.024.

Gurnell AM. 1998. The hydrogeomorphological effects of beaver dam-building activity. *Progress in Physical Geography* **22** (2): 167-189.

Hack JT. 1960. Interpretation of erosional topography in humid temperate regions. American Journal of Science **258-A**: 80–97.

Halwas KL, Church M. 2002. Channel units in small, high gradient streams on Vancouver Island, British Columbia. *Geomorphology* **43**: 243-256.

Harrison, LR, Keller EA. 2007. Modeling forced pool–riffle hydraulics in a boulder-bed stream, southern California. *Geomorphology* **83**: 232-248.

Hassan MA, Gottesfeld AS, Montgomery DR, Tunnicliffe JF, Clarke GK, Wynn G, Jones-Cox H, Poirier R, MacIsaac E, Herunter H, Macdonald SJ. 2008. Salmon-driven bed load transport and bed morphology in mountain streams. *Geophysical Research Letters* **35** (4): L04405. DOI: 10.1029/2007GL032997.

Hay GJ, Marceau DJ, Dubé P, Bouchard A. 2001. A multiscale framework for landscape analysis: Object-specific analysis and upscaling. *Landscape Ecology* **16**: 471-490. DOI: 10.1023/a:1013101931793.

Head ML, Holman L, Lanfear R, Kahn AT, Jennions MD, 2015. The extent and consequences of p-hacking in science. *PLoS Biology* **13** (3): p.e1002106. DOI: 10.1371/journal.pbio.1002106.

Ikeda S, Parker G, Sawai K. 1981. Bend theory of river meanders. Part 1. Linear development. Journal of Fluid Mechanics **112**: 363-377.

Jackson JR, Pasternack GB, Wheaton JM. 2015. Virtual manipulation of topography to test potential pool-riffle maintenance mechanisms. *Geomorphology* **228**: 617-627. http://dx.doi.org/10.1016/j.geomorph.2014.10.016

James LA. 2005. Sediment from hydraulic mining detained by Englebright and small dams in the Yuba basin. *Geomorphology* **71** (1–2): 202-226.

Jenkins G, Watts DG. 1968. Spectral analysis and its applications. Holden Day, San Francisco.

Keller EA, Florsheim JL. 1993. Velocity-Reversal Hypothesis - a Model Approach. *Earth Surface Processes and Landforms* **18**: 733-740.

Kieffer SW. 1989. Geologic Nozzles. *Reviews of Geophysics* **27**: 3-38.

Kleinhans MG. 2010. Sorting out river channel patterns. *Progress in Physical Geography* **34** (3): 287-326.

Knighton AD. 1998. Fluvial Forms and Processes: a New Perspective. Arnold, Hodder Headline, PLC.

Korup O., Schlunegger F. 2007. Bedrock landsliding, river incision, and transience of geomorphic hillslope-channel coupling: Evidence from inner gorges in the Swiss Alps. *Journal of Geophysical Research: Earth Surface* **112** (F3), F03027. DOI: 10.1029/2006JF000710

Kumar P, Foufoula-Georgiou E. 1997. Wavelet analysis for geophysical applications. *Reviews of Geophysics* **35**: 385-412. DOI: 10.1029/97RG00427.

Lane BA, Pasternack GB, Dahlke HE, Sandoval-Solis S. 2017. The role of topographic variability in river channel classification. *Physical Progress in Geography* **41** (5): 570-600. DOI: 10.1177/0309133317718133.

Legleiter CJ. 2014. A geostatistical framework for quantifying the reach-scale morphology: 1. Variogram models, related metrics, spatial structure of river and relation to channel form. *Geomorphology* **205**: 65-84.

Legleiter, CJ, Roberts DA, Lawrence RL. 2009. Spectrally based remote sensing of river bathymetry. *Earth Surface Processes and Landforms* **34** (8), 1039-1059. DOI: 10.1002/esp.1787.

Legleiter CJ, Roberts DA, Marcus WA, Fonstad MA. 2004. Passive optical remote sensing of river channel morphology and in-stream habitat; physical basis and feasibility. *Remote Sensing of Environment* **93** (4): 493-510. DOI: 10.1016/j.rse.2004.07.019.

Lenzi MA, Mao L, Comiti F. 2006. Effective discharge for sediment transport in a mountain river: Computational approaches and geomorphic effectiveness. *Journal of Hydrology* **326** (1-4): 257-276.

Leopold LB. 1962. Rivers. American Scientist **50**: 511-537.

MacWilliams ML, Wheaton JM, Pasternack GB, Kitanidis PK, Street RL. 2006. The Flow Convergence-Routing Hypothesis for Pool-Riffle Maintenance in Alluvial Rivers. *Water Resources Research* **42**: W10427. DOI: 10.1029/2005WR004391.

Molnar P, Densmore AL, McArdell BW, Turowski JM, Burlando P. 2010. Analysis of changes in the step-pool morphology and channel profile of a steep mountain stream following a large flood. *Geomorphology* **124** (1-2): 85-94.

Montgomery DR, Buffington JM, Smith RD, Schmidt KM, Pess G, 1995. Pool spacing in forest channels. *Water Resources Research* **31** (4): 1097-1105.

Moody JA, Troutman, BM. 2002. Characterization of the spatial variability of channel morphology. *Earth Surface Processes and Landforms* **27**: 1251-1266. DOI: 10.1002/esp.403.

Palmer MA, Menninger HL, Bernhardt E. 2010. River restoration, habitat heterogeneity and biodiversity: a failure of theory or practice? *Freshwater Biology* **55**: 205-222.

Palmer MA, Bernhardt ES, Allan JD, Lake PS, Alexander G, Brooks S, Carr J, Clayton S, Dahm CN, Follstad Shah J, Galat DL. 2005. Standards for ecologically successful river restoration. *Journal of Applied Ecology* **42** (2): 208-217.

Palucis MC and Lamb MP. 2017. What controls channel form in steep mountain streams? *Geophysical Research Letters* **44**: 7245–7255. DOI: 10.1002/2017GL074198.

Parker G, Izumi N. 2000. Purely erosional cyclic and solitary steps created by flow over a cohesive bed. *Journal of Fluid Mechanics* **419**: 203-238.

Passalacqua P, Belmont P, Staley DM, Simley JD, Arrowsmith JR, Bode CA, Crosby C, DeLong SB, Glenn NF, Kelly SA, Lague D., 2015. Analyzing high resolution topography for advancing the understanding of mass and energy transfer through landscapes: A review. *Earth-Science Reviews* **148**: 174-193.

Pasternack GB. 2011. 2D Modeling and Ecohydraulic Analysis. Createspace: Seattle, WA.

Pasternack GB. 2019. Applied Fluvial Ecohydraulics. Oxford Bibliographies in Environmental Science. Ed. Ellen Wohl. New York: Oxford University Press, Entry Launch Date 2019-10-30. DOI: 10.1093/OBO/9780199363445-0124.

Pasternack GB. 2020a. River Restoration: Disappointing, Nascent, Yet Desperately Needed. Reference Module in Earth Systems and Environmental Sciences. Elsevier. DOI: 10.1016/B978-0-12-409548-9.12449-2.

Pasternack GB. 2020b. Geomorphic Covariance Structures. YouTube. https://www.youtube.com/watch?v=VSMK72FbTfI.

Pasternack GB, Hinnov LA. 2003. Hydro meteorological controls on water level in a vegetated Chesapeake Bay tidal freshwater delta. Estuarine, Coastal, and Shelf Science **58** (2): 373-393.

Pasternack GB, Senter AE. 2011. 21st Century instream flow assessment framework for mountain streams. California Energy Commission, PIER. CEC-500-2013-059.

Pasternack GB, Zhang M. 2020. River Builder User's Manual For Version 1.0.0. University of California, Davis, CA.

Pasternack GB, Bounrisavong MK, Parikh KK. 2008. Backwater control on riffle-pool hydraulics, fish habitat quality, and sediment transport regime in gravel-bed rivers. *Journal of Hydrology* **357** (1-2): 125-139.

Pasternack GB, Baig D, Weber M, Brown R. 2018a. Hierarchically nested river landform sequences. Part 1: Theory. *Earth Surface Processes and Landforms* **43** (12): 2510-2518. DOI: 10.1002/esp.4411.

Pasternack, GB, Baig D, Weber M, Brown R. 2018b. Hierarchically nested river landform sequences. Part 2: Bankfull channel morphodynamics governed by valley nesting structure. *Earth Surface Processes and Landforms* **43** (12): 2519-2532. DOI: 10.1002/esp.4410.

Radecki-Pawlik A. 2002. Bankfull discharge in mountain streams: theory and practice. *Earth Surface Processes and Landforms* **27** (2): 115-123.

Roni P, Hanson K, Beechie TJ. 2008. Global review of the physical and biological effectiveness of stream habitat rehabilitation techniques. *North American Journal of Fisheries Management* **28**: 856-890.

Rosgen DL. 1996. Applied river morphology, Pagosa Springs, CO: Wildland Hydrology Books.

Rosgen DL. 2006. The natural channel design method for river restoration. In: Graham, R. (Ed.), Proceedings of the 2006 World Environmental and Water Resources Congress, May 21-25, 2006. American Society of Civil Engineers, Omaha, NE.

Sawyer AM, Pasternack GB, Moir HJ, Fulton AA. 2010. Riffle-pool maintenance and flow convergence routing observed on a large gravel-bed river. *Geomorphology* **114**: 143-160.

Scown MW, Thoms MC, De Jager NR. 2015. Measuring floodplain spatial patterns using continuous surface metrics at multiple scales. *Geomorphology* **245**: 87-101.

Sheldon F., Thoms MC. 2006. In-channel geomorphic complexity: The key to the dynamics of organic matter in large dryland rivers?. *Geomorphology* **77** (3-4), 270-285.

Simon A, Doyle M, Kondolf GM, Shields Jr. FD, Rhoads B, McPhillips M. 2008. Reply to discussion: "critical evaluation of how the Rosgen classification and associated 'natural channel design' methods fail to integrate and quantify fluvial processes and channel responses" by A. Simon, M. Doyle, M. Kondolf, F.D. Shields Jr., B. Rhoads, and M. McPhillips. *Journal of the American Water Resources Association* **44** (3): 793-802.

Sklar, L.S. Dietrich, W.E. 2006. The role of sediment in controlling steady-state bedrock channel slope: Implications of the saltation–abrasion incision model. *Geomorphology* **82** (1-2): 58-83.

Strom MA, Pasternack GB, Wyrick JR. 2016. Reenvisioning velocity reversal as a diversity of hydraulic patch behaviours. *Hydrological Processes* **30**: 2348-2365. DOI: 10.1002/hyp.10797.

Thompson DM. 2001. Random controls on semi-rhythmic spacing of pools and riffles in constriction-dominated rivers. *Earth Surface Processes and Landforms* **26**: 1195-1212.

Thompson DM, Wohl EE, Jarrett RD. 1999. Velocity reversals and sediment sorting in pools and riffles controlled by channel constrictions. *Geomorphology* **27**, 229-241.

Thoms MC. 2006. Variability in riverine ecosystems. *River Research and Applications* **22** (2): 115-121.

Thomson JR, Taylor MP, Fryirs, K. A. & Brierley, G. J. 2001. A geomorphological framework for river characterization and habitat assessment. *Aquatic Conservation-Marine and Freshwater Ecosystems*, 11, 373-389.

Tonina D, Jorde K. 2013. Hydraulic modelling approaches for ecohydraulic studies: 3D, 2D, 1D and non-numerical models. In Ecohydraulics, an integrated approach. Edited by I. Maddock, A. Harby, P. Kemp, and P. Wood, 31–74. Chichester, UK: Wiley Blackwell.

Veilleux AG, Cohn TA, Flynn KM, Mason Jr RR, Hummel PR. 2014. Estimating magnitude and frequency of floods using the PeakFQ 7.0 program: U.S. Geological Survey Fact Sheet 2013-3108, http://pubs.usgs.gov/fs/2013/3108/

Wald A, Wolfowitz J. 1940. On a test whether two samples are from the same population. *The Annals of Mathematical Statistics* **11**: 147–162.

Warfe DM, Barmuta LA, Wotherspoon S. 2008 Quantifying habitat structure: surface convolution and living space for species in complex environments. *Oikos* **117**: 1764–1773.

Wentworth CK. 1922. A scale of grade and class terms for clastic sediments. The Journal of geology **30** (5): 377-392.

Wheaton JM, Pasternack GB, Merz JE. 2004. Spawning habitat rehabilitation - 2. using hypothesis development and testing in design, Mokelumne River, California, U.S.A. *International Journal of River Basin Management* **2** (1): 21-37.

Wheaton JM, Fryirs KA, Brierley G, Bangen SG, Bouwes N, O'Brien G. 2015. Geomorphic mapping and taxonomy of fluvial landforms. *Geomorphology*, **248** (Supplement C): 273-295.

Wiener J, Pasternack GB. 2016a. Accretionary Flow Analysis- Yuba River from New Bullards Bar to Colgate Powerhouse. Prepared for Yuba County Water Agency. University of California, Davis, CA.

Wiener J, Pasternack GB. 2016b. 2014 Topographic Mapping Report- Yuba River from New Bullards Bar to Colgate Powerhouse. Prepared for Yuba County Water Agency. University of California, Davis, CA.

Wohl E, Lane SN, Wilcox AC. 2015. The science and practice of river restoration. *Water Resources Research* **51** (8): 5974-5997.

Wyrick JR, Pasternack GB. 2014. Geospatial organization of fluvial landforms in a gravel-cobble river: beyond the riffle-pool couplet. *Geomorphology* **213**: 48-65. DOI: doi:10.1016/j.geomorph.2013.12.040.

Wyrick JR, Pasternack GB. 2015. Revealing the natural complexity of topographic change processes through repeat surveys and decision-tree classification. *Earth Surface Processes and Landforms* **41**: 723-737. DOI: 10.1002/esp.3854.

Wyrick JR, Senter AE, Pasternack GB. 2014. Revealing the natural complexity of fluvial morphology through 2D hydrodynamic delineation of river landforms. *Geomorphology* **210**: 14-22.

Yuba County Water Agency. 2012. Model Report. Appendix A. Hydrology Report. Yuba River Development Project FERC Project No. 2246.

Yuba County Water Agency. 2013. Technncal Memorandum 1-1. Channel Morphology Upstream of Englebright Reservoir. Yuba River Development Project FERC Project No. 2246.

Zimmermann A, Church M. 2001. Channel morphology, gradient profiles and bed stresses during flood in a step–pool channel. *Geomorphology* **40** (3-4): 311-327.

Tables

Table 1. Pasternack et al. (2018a) geomorphic covariance analysis framework.

Objectives (O#) and their questions	Test variables	Analysis
(O1) Analyze stage-dependent structure of fluvial topographic deviation from central tendency using longitudinal series of standardized width (Ws) and detrended, standardized bed elevation (Zs) for multiple flow stages.		
(1a) What percent of the river has topographic variations greater than 0.5 and one standard deviations away from the mean?	Abs(Zs), Abs(Ws)	percent of values > 1 or > 0.5
(1b) Is longitudinal topographic structure random?	series of Zs, Ws	Wald-Wolfowitz* runs tests
(1c) Are width and bed elevation series correlated, as one indicator of coherent organization?	series of Zs, Ws	Pearson's product-moment correlation for Ws and Zs
(O2) Analysis of presence of flow convergence routing using Ws·Zs spatial series for multiple flow stages.		
(2a) At what stage and discharge, if any, does the morphological structure abruptly change from negative to positive covariance?	series of Ws·Zs	mean(Ws·Zs); percent of values > 0
(2b) What stage and discharge ranges, if any, exhibit self-sustainable morphology consistent with a dominant role for flow convergence routing?	series of Ws·Zs	mean(Ws·Zs); percent of values > 0
(O3) Analyze relative abundance and longitudinal sequencing of landforms by reach and discharge.		
(3a) What is the relative abundance of each landform for the whole river for each flow?	series of landform IDs	count and compare
(3b) How do geomorphic reaches compare in landform composition?	series of landform IDs	count and compare
(3c) How does landform abundance change with flow?	series of landform IDs	count and compare
(3d) What is the longitudinal sequencing of landforms?	series of landform IDs	count times each unit followed another
(3e) How does longitudinal sequencing change with flow?	series of landform IDs	count times each unit followed another
(O4) What is the stage-dependent, nested structure of landforms classified by their flow convergence routing potential?		
(4a) What are top five most abundant nested permutations?	nested series of landform IDs	permutation abundance analysis
(4b) For each landform at the floodprone scale, what are the top three most abundance nested permutations?	nested series of landform IDs	permutation abundance analysis
(4c) For each bankfull scale landform, what are the top two most abundant nested permutations of base flow landforms?	nested series of landform IDs	permutation abundance analysis
(4d) For each landform at the bankfull scale, what are the top two most abundant floodprone landform hosts?	nested series of landform IDs	permutation abundance analysis

*Wald and Wolfowitz (1940)

Table 2. Experimental design showing questions used from Table 1, required outcomes to corroborate study hypothesis, stage at which threshold was found (if any), and conclusion about each test's outcome.

	Values required to corroborate hypothesis*			
Table 1 ID	low stage	high stage	threshold Zs**	corroboration?
1c	negative correlation	positive correlation	4.6-7	Y
2a	negative mean Ws·Zs	positive mean Ws·Zs	4.6-7	Y
2a	< 50% XS have Ws·Zs > 0	> 50% XS have Ws·Zs > 0	4.6-7	Y
3c	more O than CP	more CP than O	2-4.6	Y
3c	more NZ than WB	more WB than NZ	9-13	Y
3d	O-NZ sequences	CP-WB sequences		N
	landform nesting expectation			
4c	baseflow WB and NZ nested within bankfull WB		n/a	mostly
4c	baseflow O and CP nested within bankfull CP		n/a	mostly

*XS means cross-section, O=oversized, CP=constricted pool, NC=normal channel, WB=wide bar, NZ=nozzle. Geometric shape delineation method presented later in the text.

**Stage below which each metric matches "low stage" criterion and above which it matches "high stage" criterion.

Table 3. Estimated discharge and flood recurrence interval values for each Zd stage.

Zs (m)	Discharge (m^3/s)	Recurrence interval
1.0	2.7	1
2.0	10.8	1.06
4.6	161	2.4
7.0	350	3.5
9.0	574	6.4
13.0	1171	16.4
17.6	2109	35.9

Table 4. Topographic variability and GCS Topographic variability and GCS metrics.

	Zd stage						
Metric	1	2	4.6	7	9	13	17.6
(A) Topographic variability metrics							
% Abs(Zs)>1	23	26	26	26	26	27	27
% Abs(Ws)>1	30	29	23	20	21	19	16
r*	-0.62	-0.50	-0.16	0.06	0.10	0.13	0.18
(B) Geomorphic covariance metrics**							
Mean Zs·Ws	-0.62	-0.50	-0.16	0.06	0.10	0.13	0.18
% Zs·Ws > 0	30	34	47	52	55	53	55

*Pearson's product-moment correlation (r) values for Ws and Zs. Blue and red shading indicate the highest and lowest values in each column. Grey shading indicates negative r-values that are not the lowest.

**Dark shading indicates values below hypothesized threshold.

Table 5. Analysis of landform composition of river as a function of flow. Light grey indicates higher abundance of each type of deep landform. Dark grey indicates higher abundance of each type of shallow landform.

	% of XS locations				
Zs	O	CP	NC	WB	NZ
1	12	1.4	62	3.3	21
2	11	2.5	65	3.8	18
4.6	5.4	8	67	7	13
7	3.7	9.6	71	6.2	10
9	4.6	10	70	7.3	7.5
13	5.4	11	70	7.1	6.0
17.6	5.3	11	71	7.1	5.7

*O=oversized, CP=constricted pool, NC=normal channel, WB=wide bar, NZ=nozzle.

Table 6. Longitudinal sequencing of landforms for the whole river, excluding normal channel units. Shading indicates values more than 10 percentage points higher than radon expectation.

	% of times unit followed the starting unit			
Starting unit	O	CP	WB	NZ
(A) Zs = 1 m				
O		40	30	30
CP	44		6	50
WB	53	13		33
NZ	30	30	40	
(B) Zs = 2 m				
O		39	44	17
CP	33		5	62
WB	62	8		31
NZ	20	65	15	
(C) Zs = 4.6 m				
O		69	31	0
CP	26		19	56
WB	40	33		27
NZ	5	63	32	
(D) Zs = 7 m				
O		56	44	0
CP	16		21	63
WB	33	39		28
NZ	6	41	53	

	% of times unit followed the starting unit			
Starting unit	O	CP	WB	NZ
(E) Zs = 9 m				
O		50	50	0
CP	18		29	53
WB	41	35		24
NZ	8	46	46	
(F) Zs = 13 m				
O		29	71	0
CP	15		25	60
WB	57	19		24
NZ	0	71	29	
(G) Zs = 17.6 m				
O		21	79	0
CP	4		23	73
WB	69	27		4
NZ	5	75	20	

Table 7. Top three permutations of hierarchical nesting of flow convergence routing landforms within the five floodprone landform types.

Zs = 9	Zs = 4.6	Zs = 1	Count	% of river
(A) Nested within floodprone nozzle				
NZ	NZ	NZ	160	5.4
NZ	NZ	NC	33	1.1
NZ	NC	NC	18	0.6
(B) Nested within floodprone wide bar				
WB	WB	NZ	52	1.8
WB	NC	NC	48	1.6
WB	NC	NZ	44	1.5
(C) Nested within floodprone normal channel				
NC	NC	NC	1161	39
NC	NC	NZ	338	11
NC	NZ	NZ	119	4.0
(D) Nested within floodprone constricted pool				
CP	NC	NC	118	4.0
CP	CP	NC	80	2.7
CP	NC	O	56	1.9
(E) Nested within floodprone oversized				
O	O	O	59	2.0
O	NC	WB	21	0.7
O	NC	NC	20	0.7

Table 8. Top two permutations of hierarchical nesting of bankfull landforms, either within (A-E) or beyond (F-J) them.

Test 1: within bankfull landform				Test 2: what each bankfull landform is nested within			
Zs = 4.6	Zs = 1	Count	% of river	Zs = 9	Zs = 4.6	Count	% of river
(A) within bankfull nozzle				(F) hosting bankfull nozzle			
NZ	NZ	293	10	NZ	NZ	193	6.6
NZ	NC	81	2.8	NC	NZ	152	5.2
(B) within bankfull wide bar				(G) hosting bankfull wide bar			
WB	NZ	109	3.7	NC	WB	111	3.8
WB	NC	78	2.7	WB	WB	69	2.3
(C) within bankfull normal channel				(H) hosting bankfull normal channel			
NC	NC	1365	46	NC	NC	1623	55.1
NC	NZ	392	13	CP	NC	182	6.2
(D) within bankfull constricted pool				(I) hosting bankfull constricted pool			
CP	NC	163	5.5	CP	CP	117	4.0
CP	O	47	1.6	NC	CP	108	3.7
(E) within bankfull oversized				(J) hosting bankfull oversized			
O	O	132	4.5	NC	O	80	2.7
O	NC	19	0.6	O	O	76	2.6

Table Captions

Table 1. Pasternack et al. (2018a) geomorphic covariance analysis framework.

Table 2. Experimental design showing questions used from Table 1, required outcomes to corroborate study hypothesis, stage at which threshold was found (if any), and conclusion about each test's outcome.

Table 3. Estimated discharge and flood recurrence interval values for each Zd stage.

Table 4. Topographic variability and GCS Topographic variability and GCS metrics.

Table 5. Analysis of landform composition of river as a function of flow. Light grey indicates higher abundance of each type of deep landform. Dark grey indicates higher abundance of each type of shallow landform.

Table 6. Longitudinal sequencing of landforms for the whole river, excluding normal channel units. Shading indicates values more than 10 percentage points higher than radon expectation.

Table 7. Top three permutations of hierarchical nesting of flow convergence routing landforms within the five floodprone landform types.

Table 8. Top two permutations of hierarchical nesting of bankfull landforms, either within (A-E) or beyond (F-J) them.

Figure Captions

Figure 1. Conceptual illustration and real example of spatial series nesting and decomposition. (a) A river cross-section with five water stages (blue lines) along with the corresponding nested topography under those stages. (b) Dry alluvial stream along Happy Canyon Road, Santa Ynez, California. Nested base flow (c) and valley-wide (e) width series can be deconstructed into sets of dozens to hundreds of periodic components (sum of top ten shown as red dashed line). (d,f) show five of the top ten individual components for each width series.

Figure 2. Approximate illustrations of contrasting flow convergence routing: (a) an alluvial river with freely self-maintaining alluvial landform diversity due to its landform nesting alone (low-flow (short arrows) nozzle (red) nested within

bankfull-flow (long arrows) wide bar (orange); low-flow constricted pool (blue) nested within bankfull-flow constricted pool) in which the locations of scour and deposition shift from low flow to high flow to remain at the locations of smallest cross-sectional area as these move around; and (b) a bedrock river whose landform diversity is not freely self-maintaining because its nesting (low-flow nozzle within bankfull-flow nozzle; low-flow oversized cross-section (black) within bankfull-flow oversized cross-section) maintains the same locations of scour and deposition across a wide range of flows, which would tend to homogenize topography. In (b) landform diversity is only maintained due to oversized coarse sediment and bedrock forcing, as the canyon walls are always narrow at the nozzle and wide at the oversized section. (c) conceptual cross-sections profiles (not exactly to scale) of all four sections in (a) and (b), including low-flow and high-flow stage lines, colored by landform type.

Figure 3. Location map of Yuba River watershed and study segment.

Figure 4. Data processing workflow and flow convergence routing landform decision tree. “Abs” is an abbreviation for absolute value. Standardization is computed as individual rectangle value minus reach-average mean value, and then this difference is divided by reach-average standard deviation value. For full details of previously published workflow steps, see Pasternack et al. (2018a).

Figure 5. Map illustrating wetted area polygons created and used in the GCS analysis. Flow is from upper left to lower right. The confluence with the Middle Yuba River is shown in the upper right.

Figure 6. Longitudinal Ws series for middle 10 km contrasting (a) lowest and (b) highest discharge.

Figure 7. Schematic illustrating the primary (thick arrows) and secondary (thin arrows) transitions between the landform types regardless of discharge contrasting (a) hypothesized and (b) observed. Bidirectional arrows indicate that this pair of landforms forms a repeating couplet.

Figure 8. Series of Ws·Zs for the lowest four stages with colors representing landform type.

Figure 9. Series of Ws·Zs for the highest three stages with colors representing landform type.

Figure 10. Sankey diagrams showing landform sequencing for Zd stages of (a) 1 m, (b) 4.6 m, and (c) 9 m. Landform types indicated by same colors as in previous figures. Left side shows upstream landform. Right side shows downstream landform.

Figure 11. Aerial images illustrating four different 3-scale nesting structures. (a) Nozzle in nozzle in nozzle (39°22'40.60"N, 121° 8'22.37"W), (b) oversized in constricted pool in constricted pool (39°19'55.64"N, 121° 9'34.89"W), (c) nozzle in nozzle in wide bar (39°21'38.33"N, 121° 8'26.74"W), (d) wide bar in wide bar in oversized (39°19'49.27"N, 121°11'22.04"W). Images are shown at different scales, so widths are not directly comparable. Flow is right to left for all images. Landform-indicating colors are the same as in all previous figures.